

Exact Stationary State of a d -dimensional Run-and-Tumble Particle in a Harmonic Potential

Mathis Guéneau,¹ Satya N. Majumdar,² and Grégory Schehr³

¹*Max-Planck-Institut für Physik komplexer Systeme, Nöthnitzer Straße 38, 01187 Dresden, Germany*

²*LPTMS, CNRS, Univ. Paris-Sud, Université Paris-Saclay, 91405 Orsay, France*

³*Sorbonne Université, Laboratoire de Physique Théorique et Hautes Energies, CNRS UMR 7589, 4 Place Jussieu, 75252 Paris Cedex 05, France*

We derive the exact nonequilibrium steady state of a run-and-tumble particle (RTP) in d dimensions confined in an isotropic harmonic trap $V(\mathbf{r}) = \mu r^2/2$, with $r = \|\mathbf{r}\|$. Rotational invariance reduces the problem to the stationary single-coordinate marginal $p_X(x)$, from which the radial distribution $p_R(r)$ and the full joint stationary density follow by explicit integral transforms. We first focus on a generalized trapped RTP in one dimension, where post-tumble velocities are drawn from an arbitrary distribution $W(v)$. Using a Kesten-type recursion, we represent its stationary position in terms of a stick-breaking (or Dirichlet) process, yielding closed-form expressions for its distribution and its moments. Specializing $W(v)$ to the projected velocity law of an isotropic RTP, we reconstruct $p_R(r)$ and the full joint distribution of all the coordinates in $d = 1, 2, 3$. In $d = 1$ and $d = 2$, the radial law simplifies to a beta distribution, while in $d = 3$, we derive closed-form expressions for $p_R(r)$ and the stationary joint distribution $P(x, y, z)$, which differ from a beta distribution. In all cases, we characterize a persistence-controlled shape transition at the turning surface $r = v_0/\mu$, where v_0 is the self-propulsion speed. We further include thermal noise characterized by a diffusion coefficient $D > 0$, showing that the stationary law is a Gaussian convolution of the $D = 0$ result, which regularizes turning-point singularities and controls the crossover between persistence- and diffusion-dominated regimes as $D \rightarrow 0$ and $D \rightarrow \infty$ respectively. All analytical predictions are systematically validated against numerical simulations.

CONTENTS

I. Introduction	2
II. Model and Main Results	3
A. Main Results	5
III. Generalized Run-and-Tumble Dynamics in one Dimension	6
A. Kesten Recursion Relation	7
B. Connection to the Stick-Breaking Representation of a Dirichlet Process	8
C. Stationary State and Moments for an Arbitrary Distribution $W(v)$	9
D. Large and Small α Behavior of the Stationary State	10
IV. Stationary State of a Run-and-Tumble Particle in 1D, 2D, and 3D	11
A. Stationary State of a One-Dimensional RTP	11
B. Stationary State of a Two-Dimensional RTP	13
C. Stationary State of a Three-Dimensional RTP	14
V. Stationary State of an RTP with $D > 0$ in 1D, 2D, and 3D	17
A. Stationary State of a One-Dimensional RTP with $D > 0$	18
1. Finite- D Shape Transition	18
2. Universal Low- D Scaling Form Around $z = \pm \frac{v_0}{\mu}$	19
B. Stationary State of a Two-Dimensional RTP with $D > 0$	20
C. Stationary State of a Three-Dimensional RTP with $D > 0$	21
VI. Stationary Distribution of a N -state RTP	22
VII. Conclusion	24
Appendices	25

A. Identities and Isotropy-Based Derivations	25
1. Derivation of $W_{\text{proj}}(v)$	25
2. Identities Between $p_X(x)$ and $p_R(r)$	25
3. Moments	27
4. Relation Between the Joint Law and the Radial Law	27
B. Moment Generating Function of the Generalized RTP	27
1. Kesten Approach	27
2. Moments in The Stationary State	28
C. Dirichlet Process	29
1. Cifarelli–Regazzini Identity for the MGF	29
D. Derivation of the Beta Distribution in $d = 2$	30
E. Stationary State Distribution for a Three-State RTP	31
References	32

I. INTRODUCTION

Confinement is the rule rather than the exception for active motion [1–12]: motile cells and synthetic swimmers navigate channels, pores, droplets, and traps, where geometric constraints compete with persistence and reshape steady-state statistics [13–19]. Trapping provides a particularly clean route to probe nonequilibrium steady states: even a single active particle violates detailed balance, and its stationary distribution can become strongly non-Boltzmann even without any interactions [19–27]. While minimal models such as the active Brownian particle (ABP) [28–31], the active Ornstein–Uhlenbeck particle (AOUP) [32, 33], and the run-and-tumble particle (RTP) [34–36] have been extensively explored, exact stationary distributions in smooth traps remain scarce beyond one dimension [37–41]. In this work, we derive the exact stationary state of a d -dimensional run-and-tumble particle in an isotropic harmonic potential, closing the gap of an exact solution in three dimensions ($d = 3$). Our results yield explicit and testable predictions for the full stationary statistics, directly comparable to experiments.

Run-and-tumble dynamics is a minimal and widely used model of bacterial motility, notably for *E. coli* [43, 44]. In its simplest implementation, an RTP performs straight runs interrupted by isotropic reorientation events and already reproduces key microscopic features of bacterial motion [45–48]. Its motion is intrinsically out of equilibrium, affecting not only steady states but also time-dependent observables, including relaxation and first-passage properties [49–65]. A harmonic trap is a natural and versatile minimal model of confinement as it describes the vicinity of a stable minimum to leading order. Experimentally, optical and acoustic tweezers are often approximated by a quadratic potential near the trapping point and provide a controlled way to manipulate individual bacteria [66–70]. Exact stationary distributions for harmonically trapped run-and-tumble particles are known in one dimension [24, 71, 72] and in a few specific two-dimensional settings [39–41, 73], whereas closed-form results in higher dimensions remain, to our knowledge, unavailable – see e.g. [41]. While one may try to obtain the stationary state from a Fokker–Planck description, for RTPs this route leads to a nonlocal integro-differential equation that does not appear analytically tractable. Here, we instead solve the problem via a different route, based on a Kesten recursion [71, 74] and its Dirichlet-process representation (via a stick-breaking construction) [75–77], which provides the stationary distribution in closed form for any dimension.

For bounded-speed dynamics such as run-and-tumble motion, confinement generically creates turning points (or, in higher dimensions, a turning surface) where the force generated from the potential exactly balances self-propulsion and the deterministic velocity vanishes [24, 54, 55, 78–80]. Near these locations, the stationary distribution undergoes a transition as the ratio between the tumbling rate and the trap relaxation rate is varied. In one dimension, this interplay is known to yield a persistence-controlled *shape transition* [24]: the stationary density crosses over from a regular, bell-shaped profile at low persistence to an active regime in which the probability mass accumulates at the turning points, producing integrable edge singularities. The structure of this transition in higher dimensions – most notably, the associated radial statistics that directly quantify accumulation near the turning surface – remains comparatively less explicit. In experimental settings, motile microorganisms are additionally subject to thermal fluctuations [45, 46], which are expected to regularize turning-point singularities, and govern the crossover between persistence-dominated and diffusion-dominated stationary regimes, motivating an explicit treatment of the combined

active and thermal noises [25].

The remainder of the paper is organized as follows. In Sec. II, we introduce the harmonically trapped RTP in d dimensions and summarize our main results, emphasizing how isotropy allows to reduce the full stationary problem to the analysis of the one-coordinate marginal. In Sec. III, we derive the stationary state of a generalized one-dimensional run-and-tumble process in a harmonic trap, where post-tumble velocities are redrawn from an arbitrary distribution. This yields an explicit stationary law for a single component of the d -dimensional RTP. In Sec. IV, we specialize these results to standard RTPs in $d = 1, 2, 3$ and compute the stationary radial distribution and the full joint distribution of the coordinates of the position, including a detailed characterization of the shape transition in each case. In Sec. V, we include thermal diffusion ($D > 0$), and show that the relative strength of active noise and thermal diffusion regularizes the turning-point singularity and controls the crossover between persistence-dominated and diffusion-dominated regimes in $d = 1, 2, 3$. Finally, in Sec. VI, we discuss a discrete N -state RTP as a further application. We conclude in Sec. VII with a discussion of the main implications of our exact results and a brief outlook on extensions and open questions.

II. MODEL AND MAIN RESULTS

We consider a run-and-tumble particle in d dimensions ($d > 1$), confined in a harmonic potential. Its position is

$$\mathbf{r}(t) = (x_1(t), x_2(t), \dots, x_d(t)) \in \mathbb{R}^d \quad (1)$$

and it evolves according to

$$\dot{\mathbf{r}}(t) = -\mu \mathbf{r}(t) + v_0 \mathbf{n}(t), \quad (2)$$

where $\mu > 0$ is the trap strength, $v_0 > 0$ the constant self-propulsion speed, and

$$\mathbf{n}(t) = (n_1(t), \dots, n_d(t)), \quad \|\mathbf{n}(t)\| = 1, \quad (3)$$

is the orientation vector. Between tumbles, $\mathbf{n}(t)$ remains constant. Tumbling events occur at a fixed rate γ such that the run durations are exponentially distributed

$$p(\tau) = \gamma e^{-\gamma\tau}. \quad (4)$$

It is convenient to introduce the dimensionless ratio of timescales

$$\alpha = \frac{\gamma}{\mu}, \quad (5)$$

which compares the mean run time $1/\gamma$ to the trap relaxation time $1/\mu$. At each tumbling event, the orientation is reset and drawn *isotropically*, i.e., uniformly over the unit sphere $S^{d-1} \subset \mathbb{R}^d$. Since both the trap and the reorientations are isotropic, the stationary state is rotationally invariant. As a result, each Cartesian component $x_i(t)$ evolves as a one-dimensional run-and-tumble process driven by the projected velocity $v(t) = v_0 n_i(t)$, whose stationary statistics are the same for all i . We therefore drop the index i and focus on a single component, whose Langevin equation reads

$$\dot{x}(t) = -\mu x(t) + v(t). \quad (6)$$

During the n^{th} run, the velocity component $v(t) = v_n$ is constant and drawn from the distribution

$$W_{\text{proj}}(v) = \frac{1}{v_0} \frac{\Gamma(\frac{d}{2})}{\sqrt{\pi} \Gamma(\frac{d-1}{2})} \left(1 - \frac{v^2}{v_0^2}\right)^{\frac{d-3}{2}}, \quad -v_0 \leq v \leq v_0, \quad (7)$$

where the index ‘‘proj’’ indicates that this is the distribution of a single coordinate projection of the vector $v_0 \mathbf{n}(t)$. In Fig. 1, we show a realization of such a process while in Appendix A 1, we derive the expression of $W_{\text{proj}}(v)$. When $d = 2$, the distribution of a single velocity component reduces to the arcsine law, while for $d = 3$ it becomes uniform:

$$W_{\text{proj}}(v) = \begin{cases} \frac{1}{\pi \sqrt{v_0^2 - v^2}}, & d = 2, \\ \frac{1}{2v_0}, & d = 3, \end{cases} \quad -v_0 \leq v \leq v_0. \quad (8)$$

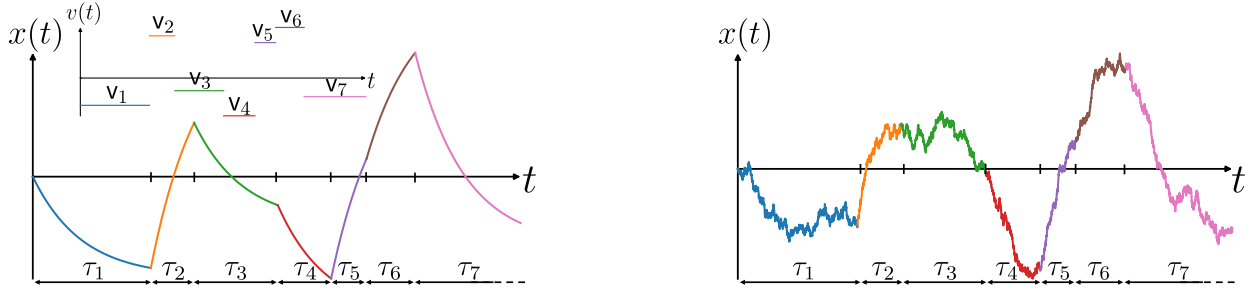


FIG. 1. Illustration of a trajectory of the generalized RTP process governed by the Langevin equation (6). **Left:** A sample trajectory for $D = 0$, where the inter-tumbling velocities v_i are drawn from an arbitrary distribution $W(v)$. **Right:** The corresponding trajectory in the presence of white noise ($D > 0$). In this case, the stationary distribution is given by the convolution of the $D = 0$ distribution with the Gaussian distribution $\mathcal{N}(0, D/\mu)$ – see Section V.

Our main goal is to determine the stationary distribution $p_R(r)$ of the particle's radial coordinate,

$$R = \|\mathbf{r}(t \rightarrow \infty)\| \stackrel{d}{=} \sqrt{x_1^2 + \dots + x_d^2}, \quad (9)$$

in arbitrary dimension d , where $x_i = x_i(t \rightarrow +\infty)$. Owing to rotational invariance, the distribution of the radius R is completely characterized by the stationary distribution $p_X(x)$ of any single coordinate, say $X \stackrel{d}{=} x_i$. The two are related through an integral transform: for $d \geq 2$,

$$p_X(x) = \frac{\Gamma(\frac{d}{2})}{\sqrt{\pi} \Gamma(\frac{d-1}{2})} \int_{|x|}^{v_0/\mu} dr \frac{p_R(r)}{r} \left(1 - \frac{x^2}{r^2}\right)^{\frac{d-3}{2}}. \quad (10)$$

The relation in Eq. (10), which is derived in Appendix A 2, expresses the coordinate distribution as a projection of the radial law and was demonstrated explicitly in [52] for the unconfined RTP. As shown in Appendix A 3, it is also possible to relate the moments of $|X|$ to those of R for any $d > 1$. In the special cases $d = 2$ and $d = 3$, the inverse relation can be obtained explicitly – see also Appendix A 2. One finds

$$p_R(r) = \begin{cases} -2r \int_r^{\frac{v_0}{\mu}} dx \frac{p'_X(x)}{\sqrt{x^2 - r^2}}, & d = 2, \\ -2r p'_X(r), & d = 3. \end{cases} \quad (11)$$

Finally, thanks to rotational invariance, the joint density of all coordinates can be expressed in terms of the radial distribution – see Appendix A 4. Specifically,

$$P(x_1, \dots, x_d) = f_R\left(r = \sqrt{x_1^2 + \dots + x_d^2}\right) = \frac{p_R(r)}{\Omega_{d-1} r^{d-1}}, \quad \Omega_{d-1} = \frac{2\pi^{d/2}}{\Gamma(d/2)}, \quad (12)$$

where Ω_{d-1} is the surface area of the unit sphere in \mathbb{R}^d .

If the RTP is additionally subjected to thermal noise, Eq. (2) acquires an additive Gaussian white-noise term, and the equation of motion becomes

$$\dot{\mathbf{r}}(t) = -\mu \mathbf{r}(t) + v_0 \mathbf{n}(t) + \sqrt{2D} \boldsymbol{\eta}(t), \quad (13)$$

where $\boldsymbol{\eta}(t) = (\eta_1(t), \dots, \eta_d(t))$ satisfies

$$\langle \eta_i(t) \rangle = 0, \quad \langle \eta_i(t) \eta_j(t') \rangle = \delta_{ij} \delta(t - t'). \quad (14)$$

For $D > 0$, the stationary position probability distribution function (PDF), denoted by $p_Z(z)$, can be expressed as the convolution of the stationary PDF in the noiseless case $D = 0$ (i.e., the Langevin dynamics (6)), denoted by $p_X(x)$, with a Gaussian distribution of mean 0 and variance D/μ . Equivalently,

$$p_Z(z) = \sqrt{\frac{\mu}{2\pi D}} \int_{-\frac{v_0}{\mu}}^{\frac{v_0}{\mu}} e^{-\frac{\mu(z-x)^2}{2D}} p_X(x) dx, \quad (15)$$

where $p_X(x)$ is supported on $[-v_0/\mu, v_0/\mu]$. This simplification follows from the linearity of Eq. (6) together with the independence of the two noise sources – see Section V. For $D > 0$, Eqs. (10)–(12) remain valid upon the replacement $p_X \rightarrow p_Z$, and the upper integration limit in Eqs. (10) and (11) is extended to $+\infty$ since $p_Z(z)$ is supported on $(-\infty, +\infty)$.

The above relations show that the stationary statistics of the d -dimensional RTP are entirely encoded in the one-coordinate marginal $p_X(x)$: once $p_X(x)$ is known, one can reconstruct the radial law $p_R(r)$, all moments, and the full joint distribution of all the coordinates. In the next section, we introduce a method to compute the stationary distribution of the Langevin dynamics (6) based on a stick-breaking (Dirichlet-process) representation. This construction yields an explicit characterization of $p_X(x)$ and thereby provides access to the complete stationary properties of the RTP. We now summarize the main results of the paper.

A. Main Results

Stationary State of a Generalized RTP. We refer to the dynamics in Eq. (6) as a generalized RTP, when at each tumble the velocity is redrawn from an arbitrary distribution $W(v)$ supported on $[v_{\min}, v_{\max}]$ – see [51]. In this case, we find that the stationary distribution of the dynamics admits an exact representation as a mean functional of a Dirichlet process [75] (equivalently, a stick-breaking construction). This yields an explicit closed-form expression for the stationary density

$$p_X(x) = \frac{1}{\pi} \int_{v_{\min}/\mu}^x dt (x-t)^{\alpha-1} \frac{d\phi_\alpha(t)}{dt}, \quad x \in \left[\frac{v_{\min}}{\mu}, \frac{v_{\max}}{\mu} \right], \quad \forall \alpha > 0, \quad (16)$$

where $\alpha = \gamma/\mu$ is given in Eq. (5) and

$$\phi_\alpha(t) = \sin \left(\pi \alpha \int_{v_{\min}}^{ut} dv W(v) \right) \exp \left(-\alpha \int_{v_{\min}}^{v_{\max}} dv \log \left| t - \frac{v}{\mu} \right| W(v) \right). \quad (17)$$

In addition, all moments $\langle X^n \rangle$ can be expressed in closed form in terms of Bell polynomials [81, 82] and the moments of $W(v)$ denoted by $\langle v^n \rangle$

$$\langle X^n \rangle = \frac{1}{\mu^n} \frac{\Gamma(\alpha)}{\Gamma(\alpha+n)} B_n \left(1! \alpha \frac{\langle v \rangle}{1}, \dots, n! \alpha \frac{\langle v^n \rangle}{n} \right). \quad (18)$$

Specializing this general result to $W_{\text{proj}}(v)$ given in Eq. (7) immediately produces the exact stationary statistics of a single coordinate of a d -dimensional RTP in a harmonic trap for any $d \geq 2$.

Stationary State in $d = 2$. Remarkably, just like in $d = 1$ [24] (see Section IV A), the stationary radial distribution simplifies to a beta distribution. In $d = 2$, this expression was previously inferred from its moments (see Refs. [39, 40])

$$p_R(r) = 2\alpha \frac{\mu^2 r}{v_0^2} \left[1 - \left(\frac{\mu r}{v_0} \right)^2 \right]^{\alpha-1}, \quad 0 \leq r \leq \frac{v_0}{\mu}. \quad (19)$$

Its edge behavior exhibits a transition at $\alpha = 1$, diverging at the boundary $r_0 = v_0/\mu$ for $\alpha < 1$ (active/persistent regime) and vanishing for $\alpha > 1$ (passive regime). In the presence of thermal noise, we show that the radial distribution is given by

$$p_R \left(\tilde{r} = \frac{\mu r}{v_0} \right) = \sqrt{\frac{2}{D\mu}} \frac{v_0^2}{\pi D} \frac{\Gamma(1+\alpha)}{\Gamma(\frac{1}{2}+\alpha)} \tilde{r} \int_{\tilde{r}}^{+\infty} \frac{d\tilde{z}}{\sqrt{\tilde{z}^2 - \tilde{r}^2}} \int_{-1}^1 d\tilde{x} (\tilde{z} - \tilde{x}) (1 - \tilde{x}^2)^{\alpha-\frac{1}{2}} e^{-\frac{v_0^2}{2D\mu}(\tilde{x}-\tilde{z})^2}. \quad (20)$$

Stationary State in $d = 3$. By contrast, a closed-form expression for the stationary radial distribution in $d = 3$ does not appear to be available in the existing literature [41]. We compute it and find that it is given by

$$p_R(r) = -\frac{\alpha e^\alpha}{2\pi} \frac{\mu^2}{v_0^2} r \left[\pi A(r)^{\alpha-1} + \int_0^{A(r)} du (A(r) - u)^{\alpha-1} f'(u) \right], \quad (21)$$

where

$$A(r) = \frac{1}{2} \left(\frac{\mu r}{v_0} + 1 \right), \quad f(u) = e^{-\alpha [u \ln u + (1-u) \ln(1-u)]} \left[\pi \cos(\pi \alpha u) - \ln \left(\frac{u}{1-u} \right) \sin(\pi \alpha u) \right]. \quad (22)$$

In $d = 3$ also, we find that the PDF $p_R(r)$ exhibits a shape transition at $\alpha = 1$, as in $d = 2$. In particular, at this transition when $\alpha = 1$, the expression simplifies to

$$p_R(r) = \frac{e \mu^2 r}{\pi v_0^2} \left(1 - \frac{\mu r}{v_0} \right)^{-\frac{1}{2} \left(1 - \frac{\mu r}{v_0} \right)} \left(1 + \frac{\mu r}{v_0} \right)^{-\frac{1}{2} \left(1 + \frac{\mu r}{v_0} \right)} \left[2 \operatorname{arctanh} \left(\frac{\mu r}{v_0} \right) \cos \left(\frac{\mu \pi r}{2 v_0} \right) + \pi \sin \left(\frac{\mu \pi r}{2 v_0} \right) \right]. \quad (23)$$

We also compute the exact radial distribution in the presence of additional thermal noise in Section [V C](#).

Thermal noise ($D > 0$) and finite- D shape transitions. When an additional Gaussian white noise of diffusivity $D > 0$ is present, the equation of motion is given in Eq. (13). This equation being linear, the stationary law is obtained by a Gaussian convolution of the $D = 0$ steady state (see Eq. (15)). This representation makes explicit how temperature (i) rounds off the turning-point singularities, (ii) generates a Gaussian tail beyond the edge of the support $r_0 = v_0/\mu$, and (iii) controls the crossover between persistence-dominated and diffusion-dominated regimes. It is convenient to quantify the relative strength of thermal fluctuations to active noise through the dimensionless parameter

$$\theta = \frac{2\mu D}{v_0^2} = \frac{2}{\alpha} \frac{D}{D_{\text{eff}}}, \quad (24)$$

where $D_{\text{eff}} = v_0^2/\gamma$ is the effective diffusion coefficient of a free RTP. As θ decreases, the stationary distribution exhibits a qualitative change: in $d = 1$ and $d = 2$ the stationary density smoothly crosses over from a unimodal profile peaked at the origin to a bimodal profile with two maxima near the turning points. In $d = 3$, the corresponding transition becomes richer, with a coexistence region in which an inner and an outer maximum compete. In some cases, the position of the global maximum jumps discontinuously from $r = 0$ to a shell near $r = r_0$ (see Fig. 10).

N -state Model. As a direct consequence of Eq. (16), one can compute the stationary state of a N -state model

$$W(v) = \sum_{i=1}^N p_i \delta(v - v_i), \quad 0 < p_i < 1, \quad \sum_{i=1}^N p_i = 1. \quad (25)$$

We find that $p_X(x)$ is the distribution of a linear combination of a Dirichlet random vector. Its expression is given by

$$p_X(x) = \frac{\Gamma(\alpha)}{\prod_{i=1}^N \Gamma(\alpha p_i)} \int_0^1 dz_1 \cdots \int_0^1 dz_N \delta \left(x - \frac{1}{\mu} \sum_{i=1}^N v_i z_i \right) \left(\prod_{i=1}^N z_i^{\alpha p_i - 1} \right) \delta \left(1 - \sum_{i=1}^N z_i \right). \quad (26)$$

In particular, it turns out that the density is piecewise continuous on the intervals $x \in]v_k/\mu, v_{k+1}/\mu[$ where $v_k < v_{k+1}$ for all $k = 1, \dots, N-1$ – see Eq. (113) and Fig. 11. If $N = 2$, $v_1 = -v_2 = v_0$ and $p_1 = p_2 = 1/2$, this corresponds to the standard one-dimensional RTP [24, 34, 83–85].

III. GENERALIZED RUN-AND-TUMBLE DYNAMICS IN ONE DIMENSION

To calculate the steady state distribution of a d -dimensional RTP, we first consider a generalized one-dimensional run-and-tumble particle evolving in a harmonic trap, starting from the initial condition $x(0) = 0$. The dynamics is governed by Eq. (6), where $v(t)$ is piecewise constant and changes only at the tumbling times (see the left panel of Fig. 1 for an example trajectory). At each tumbling event, which occurs with a fixed rate γ , the velocity v is redrawn from a prescribed distribution $W(v)$ supported on $[v_{\min}, v_{\max}]$ [51]. Importantly, in this section, we focus on a completely general $W(v)$ which may be either discrete or continuous. In particular, when the distribution $W(v)$ is chosen as in Eq. (7), the dynamics in Eq. (6) corresponds to the one of a single component of the d -dimensional RTP introduced in the previous section.

A. Kesten Recursion Relation

One way to describe the dynamics given in Eq. (6) is to consider the deterministic motion between successive tumbling times $\{t_1, t_2, \dots, t_n\}$ [71]. Introducing the variable x_n to denote the position of the particle immediately after the n -th tumbling event, we can derive a recursive relation for x_n . Indeed, integrating Eq. (6) over one run, i.e., between t_{n-1} and t_n , and defining $\tau_n = t_n - t_{n-1}$, we obtain

$$x_n = x_{n-1} e^{-\mu\tau_n} + \frac{v_n}{\mu} (1 - e^{-\mu\tau_n}), \quad x_0 = 0, \quad (27)$$

where we recall that $p(\tau_n) = \gamma e^{-\gamma\tau_n}$ and v_n is drawn from the PDF $W(v)$. This recursion has the characteristic form of a Kesten relation [71, 74],

$$x_n = U_n x_{n-1} + V_n, \quad U_n = e^{-\mu\tau_n}, \quad V_n = \frac{v_n}{\mu} (1 - U_n), \quad (28)$$

where U_n and V_n are random variables. Given that τ_n follows an exponential distribution with fixed rate γ , it is straightforward to show that $U_n \sim \text{Beta}(\alpha, 1)$, i.e.

$$P(U) = \alpha U^{\alpha-1}, \quad 0 \leq U \leq 1, \quad \alpha = \frac{\gamma}{\mu}. \quad (29)$$

The parameter α represents the ratio between the two characteristic timescales of the system: the average relaxation time of the particle within the harmonic trap, $1/\mu$, and the mean time between two tumbling events, $1/\gamma$. This important parameter effectively controls the level of activity of the particle: the smaller α is, the more persistent its motion becomes.

The stationary properties of such Kesten relations are usually studied by integrating over all paths connecting x_{n-1} to x_n under the constraint of Eq. (28). One indeed obtains [71, 74, 86, 87]

$$p_X(x, n) = \int dU \int dV \int dx' P(U, V) p(x', n-1) \delta(x - U x' - V), \quad (30)$$

where $p_X(x, n)$ is the probability distribution of the random variable x_n and $P(U, V)$ is the joint PDF of the random variables U and V . Taking the limit $n \rightarrow +\infty$ in Eq. (30), and assuming $p_X(x) = \lim_{n \rightarrow +\infty} p_X(x, n)$ exists, leads to an integral equation satisfied by the stationary distribution

$$p_X(x) = \int dU \int dV \int dx' P(U, V) p_X(x') \delta(x - U x' - V). \quad (31)$$

Since τ_n 's (hence U_n 's – see Eq. (28)) are independent of the post-tumble velocity v_n drawn from $W(v)$, the joint law factorizes as $P(U, V) = P(U) P(V|U)$. For fixed U , the change of variables $v = \mu V / (1 - U)$ yields

$$P(V|U) = \frac{\mu}{1 - U} W\left(\frac{\mu V}{1 - U}\right), \quad (32)$$

with support $V \in [(1 - U)v_{\min}/\mu, (1 - U)v_{\max}/\mu]$. Combining this result with Eq. (29) yields the joint law of U_n and V_n defined in Eq. (28), namely

$$P(U, V) = P(U) P(V|U) = \alpha U^{\alpha-1} \frac{\mu}{1 - U} W\left(\frac{\mu V}{1 - U}\right). \quad (33)$$

Therefore, the steady state distribution of the generalized RTP satisfies the following integral equation

$$p_X(x) = \int dU \int dV \int dx' \alpha U^{\alpha-1} \frac{\mu}{1 - U} W\left(\frac{\mu V}{1 - U}\right) p_X(x') \delta(x - U x' - V). \quad (34)$$

Although this integral equation is very complicated, it can be solved explicitly for the moment generating function (MGF) of X , which is defined as

$$\tilde{p}_X(q) = \langle e^{qx} \rangle = \int_{-\infty}^{+\infty} dx e^{qx} p_X(x). \quad (35)$$

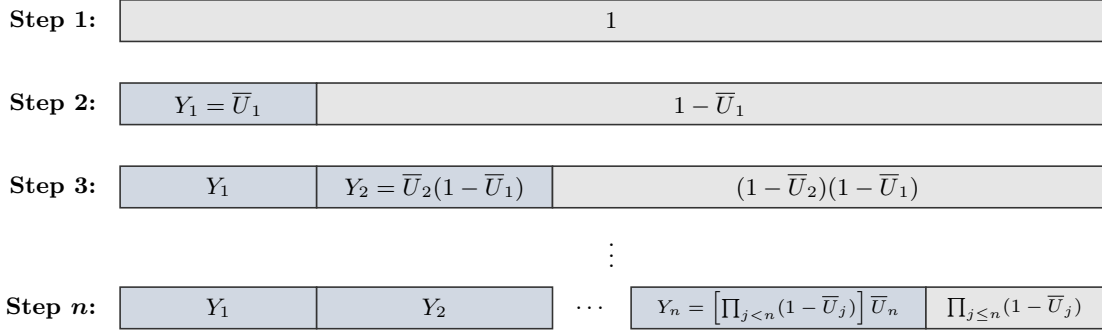


FIG. 2. Illustration of the iterative steps of a stick-breaking process, in which a stick of unit length is successively broken into infinitely many pieces from left to right. At step 1, a fraction $Y_1 = \bar{U}_1$ is removed, leaving a segment of length $1 - \bar{U}_1$. At step 2, a fraction \bar{U}_2 of the remaining stick is broken off, producing a new piece of length $Y_2 = \bar{U}_2(1 - \bar{U}_1)$ and leaving a residual segment of length $(1 - \bar{U}_2)(1 - \bar{U}_1)$. The procedure continues indefinitely, yielding pieces of lengths Y_n . Each $\bar{U}_n \in (0, 1)$ is drawn independently from a distribution Beta(1, α).

We show in Appendix B 1 that the solution for $\tilde{p}_X(q)$ reads

$$\tilde{p}_X(q) = \Gamma(\alpha) \int_{\Gamma_B} \frac{ds}{2\pi i} \exp\left(s - \alpha \int_{v_{\min}}^{v_{\max}} dv \log\left(s - \frac{v}{\mu} q\right) W(v)\right), \quad (36)$$

where Γ represents the Bromwich contour in the complex s plane. Obtaining explicitly the stationary PDF in real space is highly challenging as it involves two nontrivial tasks: (i) performing the Bromwich integral in (36) for a fixed q and (ii) inverting the transform in (35). Instead, we adopt an alternative approach by explicitly solving the Kesten recursion (28). This reveals a connection to stick-breaking processes and allows us to obtain the full stationary state $p_X(x)$ for an arbitrary distribution $W(v)$.

B. Connection to the Stick-Breaking Representation of a Dirichlet Process

The recursion relation (27) for x_n can actually be solved explicitly. Starting from $x_0 = 0$, the first iteration gives

$$x_1 = \frac{v_1}{\mu} (1 - U_1). \quad (37)$$

Using this result iteratively, we obtain for the next terms

$$\begin{aligned} x_2 &= U_2 \frac{v_1}{\mu} (1 - U_1) + \frac{v_2}{\mu} (1 - U_2), \\ x_3 &= U_3 U_2 \frac{v_1}{\mu} (1 - U_1) + U_3 \frac{v_2}{\mu} (1 - U_2) + \frac{v_3}{\mu} (1 - U_3). \end{aligned} \quad (38)$$

By induction, the general expression after n renewals reads

$$x_n = \sum_{m=1}^n \left(\prod_{j=m+1}^n U_j \right) \frac{v_m}{\mu} (1 - U_m). \quad (39)$$

Now, apply the index reversal $m' = n + 1 - m$, $j' = n + 1 - j$ and define the reversed sequences $\tilde{U}_{j'} := U_{n+1-j'}$, $\tilde{v}_{m'} := v_{n+1-m'}$. Under this change of variables, $\prod_{j=m+1}^n U_j = \prod_{j'<m'} \tilde{U}_{j'}$. Since the sum is finite, we may reorder the terms. Relabeling dummy indices (and dropping tildes) finally gives

$$x_n = \sum_{m=1}^n \left(\prod_{j<m} U_j \right) \frac{v_m}{\mu} (1 - U_m), \quad (40)$$

where, by convention, $\prod_{j<1} U_j = 1$. In the stationary limit $n \rightarrow \infty$, this yields

$$X = \sum_{m=1}^{\infty} \left(\prod_{j<m} U_j \right) \frac{v_m}{\mu} (1 - U_m) . \quad (41)$$

Finding the steady-state distribution $p_X(x)$ seems highly nontrivial, as it is expressed as an infinite sum involving a complicated function of the set of random variables $\{U_n, v_n\}$. Remarkably, we show below that by suitably rewriting this sum, one can identify a natural connection to a stick-breaking process – see Fig. 2. Let us define

$$\bar{U}_n = 1 - U_n, \quad \bar{U}_n \sim \text{Beta}(1, \alpha) \in (0, 1). \quad (42)$$

This change of variable allows us to rewrite Eq. (41) as follows

$$X = \frac{1}{\mu} \sum_{n \geq 1} v_n Y_n, \quad Y_n = \left[\prod_{j<n} (1 - \bar{U}_j) \right] \bar{U}_n, \quad (43)$$

where the random variables Y_n 's are exactly the weights of a stick-breaking process with parameter α (see again Fig. 2). As is clear from Eq. (43), the Y_n 's are not independent: they involve overlapping products of the same form $(1 - \bar{U}_j)$, and are therefore strongly correlated. By definition of the Y_n 's, one immediately finds that

$$\sum_{n=1}^{+\infty} Y_n = 1, \quad \text{with probability 1}, \quad (44)$$

since the series is telescoping. The solution (43) admits an intuitive interpretation: the stationary position X can be mapped as a weighted sum of ballistic displacements with velocity v_n over effective times Y_n/μ . This representation is purely formal, however, since the actual dynamics is non-ballistic due to the harmonic force.

The variable X defined in Eq. (43) is a mathematical object known as a mean functional of a Dirichlet process [75]. This connection is made explicit in Appendix C, where Dirichlet processes are introduced. The statistical properties of such objects have been studied in detail in the mathematical literature, in particular in Ref. [75]. The MGF given in Eq. (36) can be recovered using the so-called Cifarelli–Regazzini identity, as shown in Appendix C 1. Moreover, Ref. [75] provides the cumulative distribution of X , which can be used to obtain the exact stationary state $p_X(x)$ (see again Appendix C).

C. Stationary State and Moments for an Arbitrary Distribution $W(v)$

Using the results in Ref. [75] from Cifarelli and Regazzini, it is possible to invert the MGF in Eq. (36) back in real space. One can show (see Appendix C) that for any $W(v)$, the stationary state is given by

$$p_X(x) = \frac{1}{\pi} \int_{v_{\min}/\mu}^x dt (x - t)^{\alpha-1} \frac{d\phi_\alpha(t)}{dt}, \quad x \in \left[\frac{v_{\min}}{\mu}, \frac{v_{\max}}{\mu} \right], \quad \forall \alpha > 0, \quad (45)$$

where

$$\phi_\alpha(t) = \sin \left(\pi \alpha \int_{v_{\min}}^{ut} dv W(v) \right) \exp \left(-\alpha \int_{v_{\min}}^{v_{\max}} dv \log \left| t - \frac{v}{\mu} \right| W(v) \right). \quad (46)$$

The moments of this distribution can be expressed explicitly in terms of Bell polynomials [82]. In Appendix B 2, we show that they are given by

$$\langle X^n \rangle = \frac{1}{\mu^n} \frac{\Gamma(\alpha)}{\Gamma(\alpha + n)} B_n \left(1! \alpha \frac{\langle v \rangle}{1}, \dots, n! \alpha \frac{\langle v^n \rangle}{n} \right). \quad (47)$$

We end this subsection with two remarks:

- **The special case $\alpha = 1$.** The stationary state takes a particularly simple form when $\alpha = 1$. This corresponds to the case where the switching rate of the velocity matches the mean relaxation time inside the harmonic well. Using Eq. (45), the kernel $(x - t)^{\alpha-1}$ then simplifies straightforwardly, and after integration, the stationary state is explicitly obtained as

$$p_X(x) = \frac{\phi_1(x)}{\pi} = \frac{1}{\pi} \sin \left(\pi \int_{v_{\min}}^{\mu x} dv W(v) \right) \exp \left(- \int_{v_{\min}}^{v_{\max}} dv \log \left| x - \frac{v}{\mu} \right| W(v) \right), \quad \alpha = 1. \quad (48)$$

These explicit and general formulae in Eqs. (45), (46), (47) and (48) constitute the main results of the present paper. In the next section, we will use them to compute explicitly the stationary PDF for the RTP in a d -dimensional harmonic potential.

- **Joint statistics of the position and the velocity in the stationary state.** Besides the position X , another interesting observable is the (total) velocity $\dot{X} = -\mu X + v$ of the particle in the stationary state. In principle, using the approach presented here it is possible to compute the joint distribution of X and v , from which the joint law of X and \dot{X} can be obtained. We refer the reader to Ref. [40] for further discussions of the marginal distribution of \dot{X} in the context of the RTP in a d -dimensional harmonic potential.

D. Large and Small α Behavior of the Stationary State

It is interesting to study how $p_X(x)$ behaves in the two extreme cases $\alpha = \gamma/\mu \rightarrow 0$ (strongly active) and $\alpha \rightarrow +\infty$ (strongly passive). To quantify the crossover, we consider the mean stick-breaking weights Y_n in Eq. (43):

$$\langle Y_n \rangle = \frac{1}{1 + \alpha} \left(\frac{\alpha}{1 + \alpha} \right)^{n-1}. \quad (49)$$

Together with $\sum_{n \geq 1} Y_n = 1$, Eq. (49) implies that the sum is dominated by the first few terms for $\alpha \rightarrow 0$, while it is spread across many components for $\alpha \rightarrow +\infty$.

Small α limit (strongly active) – few dominant velocities. For small α , the first weight Y_1 is large on average, while the subsequent weights $Y_{i>1}$ decrease rapidly. As a result, the particle spends most of its stationary lifetime in a single velocity state. Therefore, the motion of the RTP effectively reduces to ballistic motion, which in the stationary state leads to a Dirac delta-function located at the fixed-point of the dynamics, i.e., $\delta(x - \frac{v}{\mu})$. Averaging over realizations then gives

$$p_X(x) \underset{\alpha \rightarrow 0}{\approx} \int_{v_{\min}}^{v_{\max}} dv W(v) \delta \left(x - \frac{v}{\mu} \right) = \mu W(\mu x). \quad (50)$$

Large α limit (strongly passive) – highly mixed environment. For large α , all Y_n 's are small on average, meaning that the particle samples many different velocity states. The environment thus becomes a highly mixed combination of values drawn from $W(v)$, and in the infinite- α limit, the stationary distribution of the RTP position x concentrates around $\langle v \rangle / \mu$. To see this, using the expressions of the moments in Eq. (47), we have

$$\langle x \rangle = \frac{\langle v \rangle}{\mu}, \quad (51)$$

while the variance of x reads

$$\langle x^2 \rangle_c = \frac{\langle v^2 \rangle_c}{\mu^2 (1 + \alpha)} \underset{\alpha \rightarrow +\infty}{\longrightarrow} 0, \quad (52)$$

where the notation $\langle \cdot \rangle_c$ denotes the cumulants of a random variable. Therefore, when $\alpha \rightarrow +\infty$, the stationary distribution becomes concentrated in the following Dirac delta function

$$p_X(x) \underset{\alpha \rightarrow +\infty}{\approx} \delta \left(x - \frac{\langle v \rangle}{\mu} \right). \quad (53)$$

It is also instructive to analyze how the stationary state converges to the Dirac delta function. In particular, one can show that the cumulants $\langle x^{2n} \rangle_c$ decrease as $1/\alpha^{n-1}$. This implies that the Dirac delta function in Eq. (53) is approached by the following Gaussian distribution, valid for $(x - \langle v \rangle)/\mu \sim O(1/\sqrt{\alpha})$, namely

$$p_X(x) \underset{\alpha \rightarrow +\infty}{\approx} \sqrt{\frac{\mu^2 \alpha}{2\pi \langle v^2 \rangle_c}} \exp\left[-\frac{\mu^2 \alpha}{2\langle v^2 \rangle_c} \left(x - \frac{\langle v \rangle}{\mu}\right)^2\right]. \quad (54)$$

Based on the asymptotic forms given in Eqs. (50) and (54), the asymptotic behavior of the moments (47), as α is varied, can also be obtained and is given by

$$\langle x^n \rangle \approx \begin{cases} \frac{\langle v^n \rangle}{\mu^n} + O(\alpha) & , \quad \alpha \ll 1, \\ \frac{\langle v \rangle^n}{\mu^n} + \frac{n(n-1)}{2} \left(\frac{\langle v \rangle}{\mu}\right)^{n-2} \frac{\langle v^2 \rangle_c}{\mu^2 \alpha} + O(\alpha^{-2}) & , \quad \alpha \gg 1. \end{cases} \quad (55)$$

Hence, at leading order, $\langle x^n \rangle$ crosses over from $\langle v^n \rangle/\mu^n$ as $\alpha \rightarrow 0$ to $\langle v \rangle^n/\mu^n$ as $\alpha \rightarrow \infty$.

IV. STATIONARY STATE OF A RUN-AND-TUMBLE PARTICLE IN 1D, 2D, AND 3D

In Section II, we introduced the d -dimensional run-and-tumble particle and showed that each of its components follows the dynamics of the generalized one-dimensional RTP discussed in Section III. In particular, we established that the stationary distribution of this generalized RTP is given by Eq. (45). Hence, in Eq. (45), by setting $v_{\min} = -v_0$, $v_{\max} = v_0$, and using the appropriate velocity distribution $W(v)$, i.e., setting $W(v) = W_{\text{proj}}(v)$ given in Eq. (7), we can directly obtain the stationary statistics of a component of a d -dimensional RTP. For example, in two and three dimensions, the projected velocity distributions read – from Eq. (7) –

$$W_{\text{proj}}(v) = \frac{1}{\pi \sqrt{v_0^2 - v^2}}, \quad |v| \leq v_0, \quad d = 2, \quad (56)$$

and

$$W_{\text{proj}}(v) = \frac{1}{2v_0}, \quad |v| \leq v_0, \quad d = 3. \quad (57)$$

Due to isotropy, all the statistical properties of the stationary state in d dimensions can be directly obtained from those of a single component. Before studying the stationary state in two and three dimensions, it is useful to first recall the results obtained in one dimension.

A. Stationary State of a One-Dimensional RTP

We first recall the simplest realization of a run-and-tumble particle in one dimension, characterized by two possible velocities $v = \pm v_0$, chosen with equal probability,

$$W(v) = \frac{1}{2} \delta(v - v_0) + \frac{1}{2} \delta(v + v_0). \quad (58)$$

This minimal two-state model has been studied in [24, 83–85]¹. In that case, the stationary distribution of the particle position is known exactly and takes the form of a beta distribution supported on the finite interval $|x| < v_0/\mu$

$$p_X(x) = \frac{\mu}{v_0} \frac{\Gamma(\frac{\alpha+1}{2})}{\sqrt{\pi} \Gamma(\frac{\alpha}{2})} \left[1 - \left(\frac{\mu x}{v_0}\right)^2\right]^{\alpha/2-1}. \quad (59)$$

¹ In Ref. [24], the mapping of parameters is given by $\gamma \rightarrow 2\gamma$, hence $\gamma/\mu \rightarrow \alpha/2$. This correspondence arises because, in the standard RTP model, each tumbling event necessarily induces a change of velocity. In contrast, in our formulation, at a tumbling event the particle remains in the same state with probability 1/2.

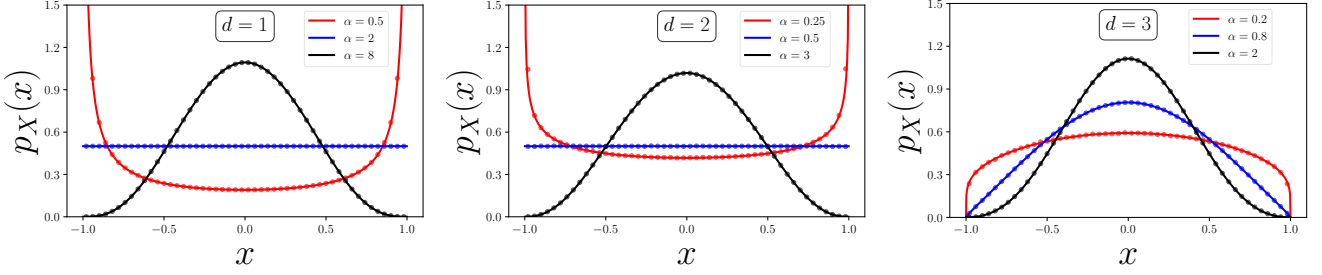


FIG. 3. Stationary probability density $p_X(x)$ of a single component of the RTP in dimensions $d = 1$ (left), $d = 2$ (center), and $d = 3$ (right), for different values of the activity parameter $\alpha = \gamma/\mu$. In $d = 1$ and $d = 2$, the distribution undergoes a shape transition at $\alpha = 2$ and $\alpha = 1/2$, respectively, signaled by the emergence or disappearance of singularities at the turning points $\pm v_0/\mu$. In contrast, in $d = 3$ the distribution remains finite and vanishes algebraically at the boundaries for all α . Solid lines are exact analytical results, while symbols correspond to numerical simulations of the RTP dynamics. Parameters are $\mu = 1$ and $v_0 = 1$.

This result can be recovered as a special case of the general N -state RTP analyzed below in Sec. VI, upon setting $N = 2$. The two edges of the support, at $\pm v_0/\mu$, correspond to the turning points of the dynamics, i.e., the positions where the velocity of the RTP vanishes. Interestingly, the stationary state exhibits a qualitative transition as the parameter α is varied. For $\alpha < 2$, corresponding to persistent motion with infrequent tumbling, the particle tends to accumulate near the turning points, leading to integrable divergences of $p_X(x)$ at the edges of the support – an “active-like” regime dominated by persistence. At the critical value $\alpha = 2$, the stationary distribution becomes uniform over the interval $[-v_0/\mu, v_0/\mu]$. In contrast, for larger values $\alpha > 2$, frequent tumbling events effectively randomize the motion, and the stationary distribution gradually approaches a Gaussian form, characteristic of a “passive-like” diffusive regime. These limiting behaviors of the stationary distribution can be made explicit through the following asymptotic forms (see Section III D)

$$p_X(x) \approx \begin{cases} \frac{1}{2} \delta\left(x - \frac{v_0}{\mu}\right) + \frac{1}{2} \delta\left(x + \frac{v_0}{\mu}\right), & \alpha \rightarrow 0, \\ \frac{\mu}{2v_0}, & \alpha = 2, \\ \frac{\mu}{v_0} \sqrt{\frac{\alpha}{2\pi}} \exp\left[-\frac{\alpha}{2} \left(\frac{\mu x}{v_0}\right)^2\right], & \alpha \rightarrow +\infty. \end{cases} \quad (60)$$

In the left panel of Fig. 3, we illustrate this shape transition and compare the analytical prediction in Eq. (59) with numerical simulations. In the following subsections, we investigate whether this shape transition of the stationary distribution, from an active-like to a passive-like form, persists in higher dimensions.

In higher dimensions, a key observable is the distribution of the radius R , i.e., the distance of the particle from the origin. For comparison, it is useful to first consider the one-dimensional case. When $d = 1$, since $R = |X|$, we have

$$p_R(r) = p_X(r) + p_X(-r) = 2p_X(r), \quad 0 \leq r \leq \frac{v_0}{\mu}. \quad (61)$$

The radial distribution exhibits the same qualitative transition as in $p_X(x)$ – see the left panel of Fig. 4. For $\alpha \rightarrow 0$, the particle is confined at the boundary $r = v_0/\mu$. For $\alpha = 2$, the distribution is uniform, while for large α , it becomes Gaussian around the origin

$$p_R(r) \approx \begin{cases} \delta\left(r - \frac{v_0}{\mu}\right), & \alpha \rightarrow 0, \\ \frac{\mu}{v_0}, & \alpha = 2, \\ \frac{\mu}{v_0} \sqrt{\frac{2\alpha}{\pi}} \exp\left[-\frac{\alpha}{2} \left(\frac{\mu r}{v_0}\right)^2\right], & \alpha \rightarrow +\infty. \end{cases} \quad (62)$$

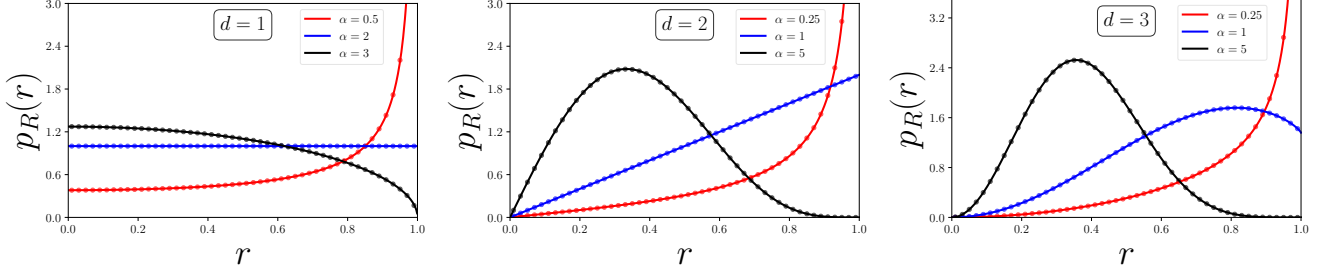


FIG. 4. Stationary radial probability density $p_R(r)$ for an RTP confined in a harmonic trap, shown for dimensions $d = 1$ (left), $d = 2$ (center), and $d = 3$ (right), and for different values of the activity parameter $\alpha = \gamma/\mu$. In all panels, we set $\mu = 1$ and $v_0 = 1$. For small α (high persistence), the probability mass accumulates near the turning radius $r = v_0/\mu$. At the critical value of α (dimension-dependent), the distribution has finite mass there. For large α (frequent tumbling), the distribution contracts toward the origin and approaches a Maxwell distribution. Solid lines are exact analytical predictions, while markers correspond to numerical simulations.

B. Stationary State of a Two-Dimensional RTP

When Eq. (45) is specialized to the arcsine distribution (56), the integrals involved can be evaluated explicitly and it is possible to show that

$$\phi_\alpha(t) = \left(\frac{2\mu}{v_0}\right)^\alpha \sin\left(\frac{\pi\alpha}{2} + \alpha \arcsin\frac{\mu t}{v_0}\right). \quad (63)$$

Consequently, for $|x| \leq v_0/\mu$, the stationary distribution reads – from Eq. (45) –

$$p_X(x) = \frac{\alpha\mu}{\pi} \left(\frac{2\mu}{v_0}\right)^\alpha \int_{-\frac{v_0}{\mu}}^x dt \frac{(x-t)^{\alpha-1}}{\sqrt{v_0^2 - \mu^2 t^2}} \cos\left(\frac{\pi\alpha}{2} + \alpha \arcsin\frac{\mu t}{v_0}\right). \quad (64)$$

Surprisingly, the integral can be evaluated exactly, and we show in Appendix D that the stationary state reduces to a beta distribution

$$p_X(x) = \frac{\mu}{v_0} \frac{\Gamma(1+\alpha)}{\sqrt{\pi} \Gamma(1/2+\alpha)} \left[1 - \left(\frac{\mu x}{v_0}\right)^2\right]^{\alpha-1/2}, \quad |x| < \frac{v_0}{\mu}. \quad (65)$$

Our result coincides with that of Ref. [39], obtained independently using a different approach, namely a Fokker–Planck approach. The stationary distribution exhibits the same asymptotic behaviors as in Eq. (60), although the transition between the active-like and passive-like regimes now occurs at $\alpha = 1/2$ – see the middle panel of Fig. 3 for a comparison with simulations. This shows that the shape transition identified in one dimension persists in the single-component dynamics of the two-dimensional RTP in the presence of a harmonic trap.

We now turn to the stationary distribution of the radius $R = \sqrt{x^2 + y^2}$. From Eq. (11), we see that it can be obtained directly from the single-component stationary state. Interestingly, it again takes the form of a beta distribution, but with a different exponent and an additional linear prefactor

$$p_R(r) = -2r \int_r^{\frac{v_0}{\mu}} dx \frac{p'_X(x)}{\sqrt{x^2 - r^2}} = 2\alpha \frac{\mu^2 r}{v_0^2} \left[1 - \left(\frac{\mu r}{v_0}\right)^2\right]^{\alpha-1}, \quad 0 \leq r \leq \frac{v_0}{\mu}. \quad (66)$$

In contrast to the one-dimensional case, the transition of the radial distribution $p_R(r)$ in two dimensions occurs at a different value of α than the transition of the single-component distribution $p_X(x)$. While $p_X(x)$ changes behavior at $\alpha = 1/2$, the radial distribution $p_R(r)$ undergoes its transition at $\alpha = 1$: for $\alpha < 1$, $p_R(r)$ diverges at the edge $r = v_0/\mu$, whereas for $\alpha > 1$ it vanishes there (see the middle panel of Fig. 4). At the critical point $\alpha = 1$, the distribution becomes linear in r near the origin. These features are made explicit by computing the behavior close to the boundary $r = v_0/\mu$. Writing $r = v_0/\mu - \epsilon$ with $\epsilon \rightarrow 0^+$, one finds

$$p_R(r) = \alpha \left(\frac{2\mu}{v_0}\right)^\alpha \epsilon^{\alpha-1} (1 + O(\epsilon)). \quad (67)$$

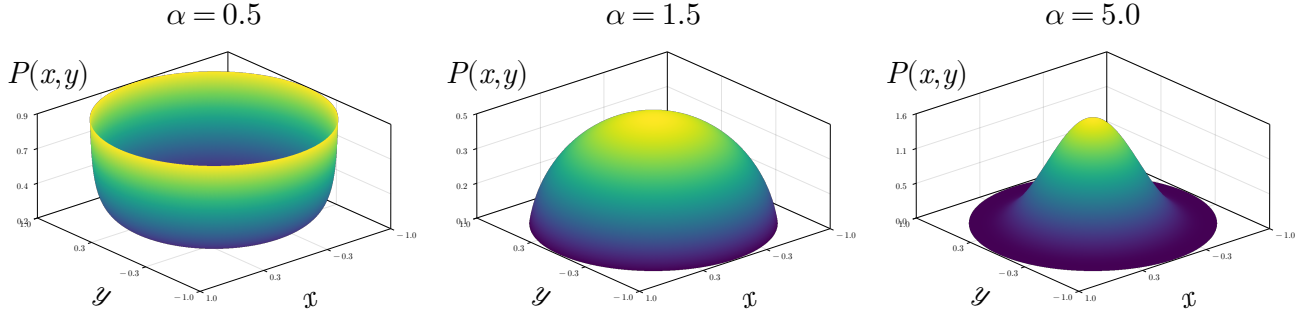


FIG. 5. Stationary joint distribution $P(x,y)$ of the RTP in $d = 2$, shown for increasing values of the activity parameter α . For $\alpha < 1$, the probability is concentrated near the turning circle $r = v_0/\mu$. At the critical point $\alpha = 1$, the density becomes uniform along the circle. For $\alpha > 1$, the distribution progressively contracts toward the origin, approaching a Gaussian form in the passive limit. Parameters are $\mu = 1$ and $v_0 = 1$.

As α is varied, $p_R(r)$ interpolates between the following asymptotic forms

$$p_R(r) \approx \begin{cases} \delta\left(r - \frac{v_0}{\mu}\right), & \alpha \rightarrow 0, \\ \frac{2\alpha\mu^2}{v_0^2}r, & \alpha = 1, \\ \frac{2\alpha\mu^2}{v_0^2}r \exp\left[-\alpha\left(\frac{\mu r}{v_0}\right)^2\right], & \alpha \rightarrow +\infty. \end{cases} \quad (68)$$

From Eq. (12), the corresponding two-dimensional stationary distribution then follows as (see also [39])

$$P(x,y) = f_R\left(r = \sqrt{x^2 + y^2}\right) = \frac{p_R(r)}{2\pi r} = \frac{\alpha\mu^2}{\pi v_0^2} \left[1 - \left(\frac{\mu r}{v_0}\right)^2\right]^{\alpha-1}, \quad 0 \leq r \leq \frac{v_0}{\mu}. \quad (69)$$

This shows that the density is maximal at the boundary for $\alpha < 1$, becomes flat at $\alpha = 1$, and concentrates near the origin for $\alpha > 1$. In particular, the stationary state interpolates continuously between an “active” regime where the particle spends most of its time at the turning circle $r = v_0/\mu$, and a “passive” regime dominated by frequent reorientations – see Fig. 5. It is thus a two-dimensional generalization of the shape transition discussed in Ref. [24].

C. Stationary State of a Three-Dimensional RTP

For a three-dimensional RTP, the projected velocity of a given component is piecewise constant and uniformly distributed over the interval $[-v_0, v_0]$. In this case, it is also possible to compute the stationary state of the individual component from Eq. (45). For x in the range $-v_0/\mu < x < v_0/\mu$, the distribution $p_X(x)$ is given by

$$p_X(x) = \frac{\alpha e^\alpha}{2\pi} \frac{\mu}{v_0} \int_0^{\frac{1}{2}(1+\frac{\mu x}{v_0})} du \left[\frac{1}{2} \left(1 + \frac{\mu x}{v_0}\right) - u \right]^{\alpha-1} f(u), \quad (70)$$

where

$$f(u) = \frac{1}{\alpha} \frac{d}{du} \left[\sin(\pi\alpha u) e^{-\alpha[u \ln u + (1-u) \ln(1-u)]} \right] = e^{-\alpha[u \ln u + (1-u) \ln(1-u)]} \left[\pi \cos(\pi\alpha u) - \ln\left(\frac{u}{1-u}\right) \sin(\pi\alpha u) \right]. \quad (71)$$

In general, it is difficult to perform explicitly the integral over u in Eq. (70). However its moments can be explicitly computed from the formula (47) leading to

$$\langle X^n \rangle = \frac{1}{\mu^n} \frac{\Gamma(\alpha)}{\Gamma(\alpha+n)} B_n \left(1! \alpha \frac{\langle v \rangle}{1}, \dots, n! \alpha \frac{\langle v^n \rangle}{n} \right), \quad \langle v^n \rangle = \frac{v_0^n}{2(n+1)} [1 + (-1)^n]. \quad (72)$$

We have explicitly checked that this formula yields back the results up to $\langle X^{10} \rangle$ given in Table I of Ref. [40].

Interestingly, in the special case $\alpha = 1$ [see also Eq. (48)] it is possible to compute explicitly the stationary distribution in (70), yielding

$$p_X(x) = \frac{e}{\pi} \frac{\mu}{v_0} \cos\left(\frac{\mu\pi x}{2v_0}\right) \left(1 + \frac{\mu x}{v_0}\right)^{-(1+\frac{\mu x}{v_0})/2} \left(1 - \frac{\mu x}{v_0}\right)^{-(1-\frac{\mu x}{v_0})/2}, \quad -\frac{v_0}{\mu} \leq x \leq \frac{v_0}{\mu}. \quad (73)$$

In Ref. [41], it was shown that $p_X(x)$ satisfies an integro-differential equation, namely

$$0 = -p_X(x) \frac{v_0}{2} \ln\left(\frac{v_0/\mu + x}{v_0/\mu - x}\right) - \frac{v_0}{2} \text{PV} \int_{-v_0/\mu}^{v_0/\mu} \frac{p_X(x')}{x - x'} dx' - \frac{v_0^2}{\mu} p'_X(x), \quad (74)$$

which was however not solved there. In fact, as also noticed in [41], this equation is similar to, though different from, the type of integral equations encountered in random matrix theory and related Coulomb gas systems [88]. However, the standard techniques to solve such equations, like Tricomi's formula, can not be used straightforwardly here, and such equations are thus difficult to solve. Here, we have checked numerically that $p_X(x)$ given in Eq. (73) indeed satisfies the integro-differential equation (74).

For general $\alpha > 0$, it is instructive to examine the behavior of $p_X(x)$ in (70) near the turning points $\pm v_0/\mu$. This allows us to address two questions: (i) whether a shape transition still occurs in three dimensions, as in $d = 1$ and $d = 2$, and (ii) whether the rather involved expression (70) eventually reduces to a simple beta distribution, as it did in lower dimensions. Since the distribution is symmetric, it is sufficient to analyze the behavior near the left boundary at $x = -v_0/\mu$. Let $\epsilon > 0$ and write $x = -v_0/\mu + \epsilon$. With the change of variable $v = u \frac{2v_0}{\mu\epsilon}$, Eq. (70) becomes

$$p_X(x) = \frac{\alpha e^\alpha}{2\pi} \frac{\mu}{v_0} \left(\frac{\mu\epsilon}{2v_0}\right)^\alpha \int_0^1 dv (1-v)^{\alpha-1} f\left(\frac{\mu\epsilon}{2v_0}v\right), \quad (75)$$

For small argument, the function $f(u)$ admits the expansion

$$f(u \rightarrow 0) \approx \pi + u[-2\pi\alpha \ln u + \pi\alpha]. \quad (76)$$

Using this expansion, one finds that for x close to either turning point, $|x| = |v_0/\mu - \epsilon|$, the stationary distribution behaves as

$$p_X(x) \approx \frac{e^\alpha}{2} \frac{\mu}{v_0} \left(\frac{\mu|\epsilon|}{2v_0}\right)^\alpha - \frac{\alpha e^\alpha}{\alpha+1} \frac{\mu}{v_0} \left(\frac{\mu|\epsilon|}{2v_0}\right)^{\alpha+1} \left[\ln\left(\frac{\mu|\epsilon|}{2v_0}\right) + \frac{1}{2} - \gamma_E - \psi(\alpha+2) \right], \quad (77)$$

where γ_E is the Euler constant and $\psi(x)$ is the digamma function. We first observe that, here, no shape transition occurs for the PDF of the projected component: as $\epsilon \rightarrow 0$, the distribution $p_X(x)$ always vanishes at the turning points, in contrast with the one- and two-dimensional cases. Moreover, the logarithmic correction appearing at the next order clearly signals a more intricate behavior than a simple beta law. Hence, already at the level of a single component, the three-dimensional case departs qualitatively from lower dimensions.

The absence of a shape transition for the projected component is further confirmed by the asymptotic forms of the distribution that one can compute using the result of Section III D. One finds

$$p_X(x) \approx \begin{cases} \frac{\mu}{2v_0}, & \alpha \rightarrow 0, \\ \sqrt{\frac{3\mu^2\alpha}{2\pi v_0^2}} \exp\left[-\frac{3\mu^2\alpha}{2v_0^2}x^2\right], & \alpha \rightarrow +\infty. \end{cases} \quad (78)$$

Thus, neither the uniform limit ($\alpha \rightarrow 0$) nor the Gaussian limit ($\alpha \rightarrow \infty$) exhibits the edge divergence characteristic of $d = 1$ and $d = 2$. These analytical predictions are fully consistent with numerical simulations, as shown in the right panel of Fig. 3.

Using isotropy, one can deduce the distribution of the radius $R = \sqrt{x^2 + y^2 + z^2}$ from $p_X(x)$ using the formula given in Eq. (11), i.e.,

$$p_R(r) = -2r p'_X(r). \quad (79)$$

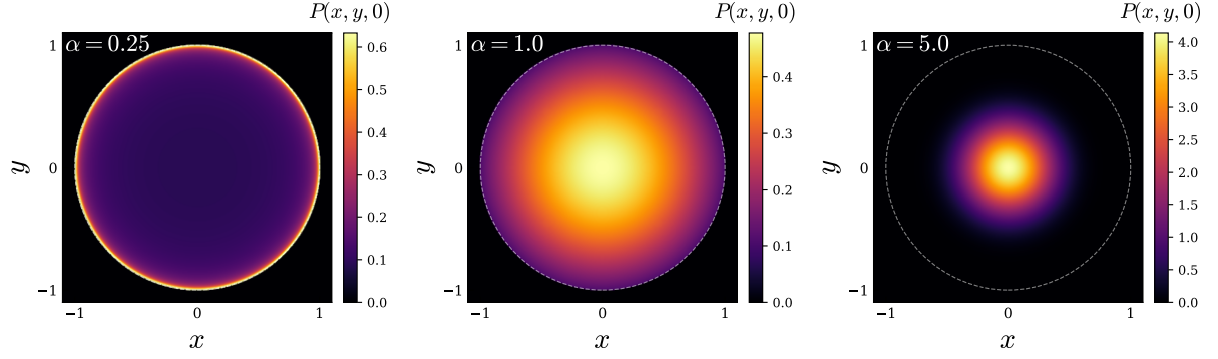


FIG. 6. Cross sections of the stationary density $P(x, y, 0)$ of a three-dimensional run-and-tumble particle for selected values of the parameter α . The distribution is supported on the sphere of radius v_0/μ and is obtained from the exact result given in Eq. (85). For small α , the density accumulates near the boundary because of the high persistence. For $\alpha \sim 1$, it becomes broad and nearly flat, and for large α , it develops a peak at the origin.

It is convenient to introduce the notation $A(x) = \frac{1}{2} \left(\frac{\mu x}{v_0} + 1 \right)$ and, with the change of variable $t = A(x) - u$, we can rewrite

$$p_X(x) = \frac{\alpha e^\alpha}{2\pi} \frac{\mu}{v_0} \int_0^{A(x)} dt t^{\alpha-1} f(A(x) - t). \quad (80)$$

Applying Leibniz's rule gives

$$p'_X(x) = \frac{\alpha e^\alpha}{2\pi} \frac{\mu}{v_0} A'(x) \left[A(x)^{\alpha-1} f(0) + \int_0^{A(x)} dt t^{\alpha-1} f'(A(x) - t) \right]. \quad (81)$$

Returning to the u -variable and noting that $f(0) = \pi$, we obtain

$$p'_X(x) = \frac{\alpha e^\alpha}{2\pi} \frac{\mu}{v_0} A'(x) \left[\pi A(x)^{\alpha-1} + \int_0^{A(x)} du (A(x) - u)^{\alpha-1} f'(u) \right]. \quad (82)$$

In the end, the radial distribution reads

$$p_R(r) = -\frac{\alpha e^\alpha}{2\pi} \frac{\mu^2}{v_0^2} r \left[\pi A(r)^{\alpha-1} + \int_0^{A(r)} du (A(r) - u)^{\alpha-1} f'(u) \right]. \quad (83)$$

As α is varied, $p_R(r)$ interpolates between the following behaviors

$$p_R(r) \approx \begin{cases} \delta\left(r - \frac{v_0}{\mu}\right), & \alpha \rightarrow 0, \\ \frac{e}{2\pi} \frac{\mu^2}{v_0^2} r |f(A(r))|, & \alpha = 1, \\ \sqrt{\frac{2}{\pi}} \left(\frac{3\mu^2 \alpha}{v_0^2} \right)^{3/2} r^2 \exp\left(-\frac{3\mu^2 \alpha}{2v_0^2} r^2\right), & \alpha \rightarrow +\infty, \end{cases} \quad (84)$$

where we recall that $A(r) = \frac{1}{2} \left(\frac{\mu r}{v_0} + 1 \right)$, while $f(u)$ is defined in Eq. (71) and is negative for $u \in [1/2, 1]$. Hence, in contrast to the component distribution, *the radial distribution does exhibit a shape transition*. For small α (high persistence), the probability mass accumulates near the spherical shell of radius v_0/μ , while for large α the density is concentrated close to the origin. The transition occurs at $\alpha = 1$, where the distribution remains finite at the turning point. For $\alpha > 1$, the radial distribution instead vanishes at the boundary. Thus, although each Cartesian component behaves differently from the one- and two-dimensional cases, the radial distribution in three dimensions

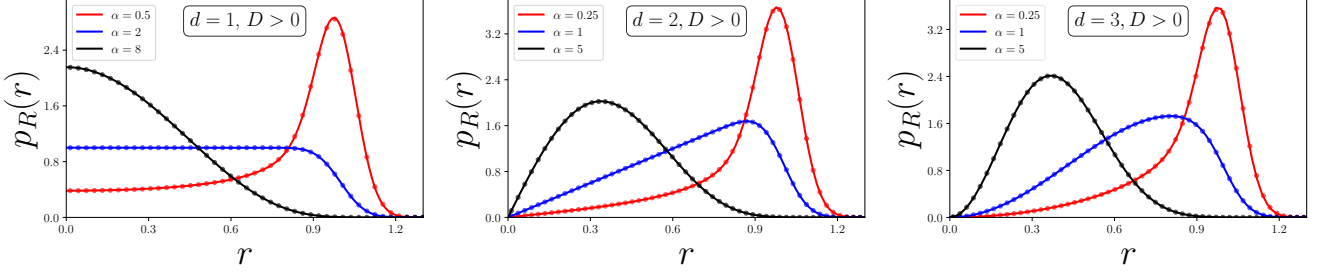


FIG. 7. Stationary radial probability density $p_R(r)$ for an RTP confined in a harmonic trap with thermal noise ($D > 0$), shown for dimensions $d = 1$ (left), $d = 2$ (center), and $d = 3$ (right). Parameters are $\mu = 1$, $v_0 = 1$, and $D = 0.005$, for different values of the parameter $\alpha = \gamma/\mu$. The presence of white noise smooths the singularities characteristic of the noiseless limit and extends the support of the distribution beyond the turning point $r_0 = v_0/\mu$. Solid lines correspond to the theoretical predictions, and markers represent Langevin simulations.

is qualitatively similar to its two-dimensional counterpart.

Finally, the joint distribution of the three components (x, y, z) is obtained using the result given in Eq. (12). It yields

$$P(x, y, z) = f_R\left(r = \sqrt{x^2 + y^2 + z^2}\right) = \frac{p_R(r)}{4\pi r^2} = -\frac{\alpha e^\alpha}{8\pi^2 r} \frac{\mu^2}{v_0^2} \left[\pi A(r)^{\alpha-1} + \int_0^{A(r)} du (A(r) - u)^{\alpha-1} f'(u) \right], \quad (85)$$

which does not reduce to a beta distribution. In Fig. 6, we plot cross sections $P(x, y, z = 0)$ for different values of α as a function of (x, y) : this shows qualitatively different behaviors as α crosses the “critical” value $\alpha = 1$ where the shape transition occurs.

V. STATIONARY STATE OF AN RTP WITH $D > 0$ IN 1D, 2D, AND 3D

We now consider a generalized run-and-tumble particle evolving in a harmonic potential and driven in addition by a thermal white noise with a diffusion coefficient D . We denote by $z(t)$ its position, whose dynamics thus reads

$$\dot{z}(t) = -\mu z(t) + v(t) + \sqrt{2D} \eta(t), \quad z(0) = 0, \quad (86)$$

where $\mu > 0$ is the trap stiffness, and $\eta(t)$ is a standard white noise with $\langle \eta(t) \rangle = 0$ and $\langle \eta(t) \eta(t') \rangle = \delta(t - t')$. The velocity $v(t)$ is again piecewise constant and takes values v_i ’s drawn from a distribution $W(v)$ with support $[v_{\min}, v_{\max}]$ between tumbling events. If one considers the pure generalized RTP $x(t)$ evolving via Eq. (6) with the *same* $v(t)$, i.e.,

$$\dot{x}(t) = -\mu x(t) + v(t), \quad x(0) = 0, \quad (87)$$

it is easy to see that the variable $y(t) = z(t) - x(t)$ is a simple Ornstein-Uhlenbeck process, namely

$$\dot{y}(t) = -\mu y(t) + \sqrt{2D} \eta(t), \quad y(0) = 0. \quad (88)$$

Since the noises $v(t)$ and $\eta(t)$ are independent, it is clear that the two random variables $x(t)$ and $y(t)$ are statistically independent, at all time t , including in the stationary state. Therefore, in the limit $t \rightarrow \infty$, one has $z(t) = x(t) + y(t)$ where the stationary distribution of $x(t)$ has been studied in Section III, and its distribution is given by $p_X(x)$ given in Eq. (45), while the distribution of $y(t)$, at large time t is simply a Gaussian of zero mean and variance D/μ . It follows from this argument that the stationary distribution of $z(t)$ is given by the convolution

$$p_Z(z) = \sqrt{\frac{\mu}{2\pi D}} \int_{\frac{v_{\min}}{\mu}}^{\frac{v_{\max}}{\mu}} e^{-\frac{\mu(z-x)^2}{2D}} p_X(x) dx. \quad (89)$$

The same convolution argument holds for the stationary distribution of the d -dimensional position vector $\mathbf{r}(t \rightarrow +\infty) = (x_1, \dots, x_d)$ in Eq. (13), but not for its norm. In the following, we will apply this formula (89) to study the standard RTP in the presence of thermal noise in $d = 1$ and higher dimensions $d > 1$ separately.

A. Stationary State of a One-Dimensional RTP with $D > 0$

In the one-dimensional case ($d = 1$), the stationary position distribution $p_Z(z)$ is the convolution of the $D = 0$ RTP density $p_X(x)$ – given in Eq. (59) – with the Gaussian distribution of zero mean and variance D/μ . By substituting the expression for $p_X(x)$ into Eq. (89), one obtains the exact stationary state for non-zero temperature (see also [25])

$$p_Z(z) = \frac{\mu}{v_0} \frac{\Gamma(\frac{\alpha+1}{2})}{\sqrt{\pi} \Gamma(\frac{\alpha}{2})} \sqrt{\frac{\mu}{2\pi D}} \int_{-\frac{v_0}{\mu}}^{\frac{v_0}{\mu}} e^{-\frac{\mu(z-x)^2}{2D}} \left[1 - \left(\frac{\mu x}{v_0} \right)^2 \right]^{\alpha/2-1} dx. \quad (90)$$

We note that in $d = 1$, the radial distribution $p_R(r)$ is simply related to the position distribution via $p_R(r) = 2p_Z(r)$ (since $R = |Z|$ – see Eq. (61)). In Fig. 7, we show a comparison of our theoretical prediction (90) with numerical simulations, showing a very good agreement. It is instructive to introduce the dimensionless scaling variables $\tilde{z} = \mu z/v_0$ and $\tilde{x} = \mu x/v_0$. In terms of these variables, Eq. (90) can be recast in the following scaling form

$$p_Z(z) = \frac{\mu}{v_0} f_\theta \left(\tilde{z} = \frac{\mu z}{v_0} \right), \quad f_\theta(\tilde{z}) = \frac{\Gamma(\frac{\alpha+1}{2})}{\pi \Gamma(\frac{\alpha}{2})} \frac{1}{\sqrt{\theta}} \int_{-1}^1 d\tilde{x} (1 - \tilde{x}^2)^{\frac{\alpha}{2}-1} e^{-\frac{(\tilde{x}-\tilde{z})^2}{\theta}}, \quad (91)$$

Here, we have introduced the dimensionless parameter θ , which quantifies the relative strength of thermal fluctuations to active noise (see Eq. (24))

$$\theta = \frac{2\mu D}{v_0^2} = \frac{2}{\alpha} \frac{D}{D_{\text{eff}}}, \quad (92)$$

where $D_{\text{eff}} = v_0^2/\gamma$ denotes the effective diffusion coefficient of a free RTP with tumbling rate γ . For sufficiently small values of θ , the shape of the distribution $p_Z(z)$ depends strongly on α . For $\alpha > 2$, the system exhibits a passive-like regime where the distribution is a unimodal, bell-shaped function centered at $z = 0$. In contrast, for $\alpha < 2$, the distribution undergoes a shape transition, exhibiting bimodality with two maxima near the boundaries of the active domain, $z = \pm v_0/\mu$ (see Fig. 8). Interestingly, a very similar shape transition of the stationary distribution $p_Z(z)$ given in Eq. (90), was also found in Ref. [89], albeit in a different context. There, the authors studied a (passive) Brownian particle in a harmonic trap whose center undergoes a telegraphic (dichotomous) process. The corresponding Langevin dynamics of that model turns out to be equivalent to Eq. (86) when $d = 1$.

One can easily derive the asymptotic behaviors of the scaling function $f_\theta(\tilde{z})$ in Eq. (91). At small \tilde{z} , the function approaches a constant, whereas for large \tilde{z} it has a Gaussian tail with a polynomial prefactor that is determined by noticing that when $\tilde{z} \rightarrow +\infty$, the integral in Eq. (91) is dominated by \tilde{x} close to 1. More precisely, one obtains

$$f_\theta(\tilde{z}) \sim \begin{cases} \frac{1}{\sqrt{\pi\theta}} {}_1F_1\left(\frac{1}{2}; \frac{\alpha+1}{2}; -\frac{1}{\theta}\right), & \text{when } \tilde{z} \rightarrow 0, \\ \frac{\Gamma(\frac{\alpha+1}{2})}{2\pi} \theta^{\frac{\alpha-1}{2}} \tilde{z}^{-\frac{\alpha}{2}} e^{-\frac{(\tilde{z}-1)^2}{\theta}}, & \text{when } \tilde{z} \rightarrow +\infty. \end{cases} \quad (93)$$

A plot of $p_R(r) = \frac{2\mu}{v_0} f_\theta \left(\frac{\mu r}{v_0} \right)$ is shown in the left panel of Fig. 7 for $r \geq 0$.

1. Finite- D Shape Transition

As D (or equivalently θ) is decreased, the scaling function exhibits qualitatively different behaviors depending on whether $\alpha > 2$ or $\alpha < 2$ (see Fig. 8). For $\alpha > 2$, the point $\tilde{z} = 0$ remains the unique maximum of $f_\theta(\tilde{z})$, and the function retains a standard bell-shaped profile for all values of θ . In contrast, for $\alpha < 2$, the origin $\tilde{z} = 0$ is a local maximum when θ is large, but becomes a local minimum when $\theta < \theta_c$, where θ_c denotes a critical value. In this regime, a peak develops away from the origin. As in Ref. [89], to determine the critical temperature $\theta_c(\alpha)$ where this transition occurs, we analyze the curvature of the scaling function at the origin, i.e., the sign of the second derivative of $f_\theta(\tilde{z})$ at $\tilde{z} = 0$. We start by expanding the exponential term in the integrand of Eq. (91) for small \tilde{z} . Using the identity $e^{-(\tilde{x}-\tilde{z})^2/\theta} = e^{-\tilde{x}^2/\theta} e^{(2\tilde{x}\tilde{z}-\tilde{z}^2)/\theta}$, we expand up to second order in \tilde{z} to get

$$e^{-\frac{(\tilde{x}-\tilde{z})^2}{\theta}} \approx e^{-\frac{\tilde{x}^2}{\theta}} \left[1 + \frac{1}{\theta} (2\tilde{x}\tilde{z} - \tilde{z}^2) + \frac{1}{2\theta^2} (2\tilde{x}\tilde{z})^2 + \mathcal{O}(\tilde{z}^3) \right]. \quad (94)$$

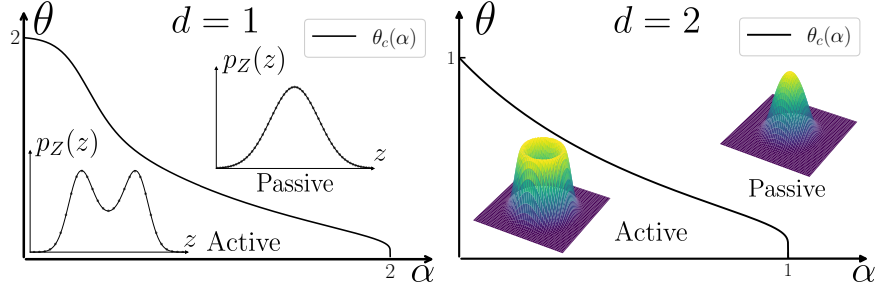


FIG. 8. Diagrams in the (α, θ) plane distinguishing between active and passive regimes for $d = 1$ (left panel) and $d = 2$ (right panel). The critical boundary $\theta_c(\alpha)$ is computed numerically using Eq. (96) for $d = 1$ and using Eq. (103) for $d = 2$. **Left:** Insets display the stationary density $p_Z(z)$ for representative parameters in the active regime ($\theta = 0.25, \alpha = 0.5$, bottom left) and the passive regime ($\theta = 4, \alpha = 2$, top right). Solid lines correspond to the exact theoretical prediction from Eq. (90), while dots represent numerical simulation results. **Right:** Surface plots of the 2D distributions generated using the analytical prediction in Eq. (102). Here the parameters used are $\theta = 0.1, \alpha = 0.5$ in the active regime (bottom left) and $\theta = 0.1, \alpha = 2$ in the passive regime (top right).

Substituting this expansion into the definition of $f_\theta(\tilde{z})$ and collecting the terms of order $\mathcal{O}(\tilde{z}^2)$, we obtain the second derivative of the scaling function at the origin

$$f_\theta''(0) = \frac{2}{\pi} \frac{\Gamma(\frac{\alpha+1}{2})}{\Gamma(\frac{\alpha}{2})} \frac{1}{\theta^{3/2}} \int_{-1}^1 dx (1-x^2)^{\frac{\alpha}{2}-1} e^{-\frac{x^2}{\theta}} \left(\frac{2x^2}{\theta} - 1 \right). \quad (95)$$

The shape transition corresponds to the point where the convexity at the origin changes sign, i.e., $f_{\theta_c}''(0) = 0$ [89]. This yields the following implicit equation for the critical temperature $\theta_c(\alpha)$ with $\alpha < 2$

$$\int_{-1}^1 dx (1-x^2)^{\frac{\alpha}{2}-1} e^{-\frac{x^2}{\theta_c(\alpha)}} \left(\frac{2x^2}{\theta_c(\alpha)} - 1 \right) = 0. \quad (96)$$

From this equation, one can obtain the asymptotic behaviors of $\theta_c(\alpha)$ in the two limits $\alpha \rightarrow 0$ and $\alpha \rightarrow 2$. In the limit $\alpha \rightarrow 0$, because of the function $(1-x^2)^{\alpha/2-1}$ the integral over x is dominated by the boundaries $x \rightarrow \pm 1$. Evaluating the integrand at these boundaries leads to the condition $2/\theta_c(0) - 1 = 0$, yielding $\theta_c(0) = 2$. In the other limit $\alpha \rightarrow 2$, a careful asymptotic analysis of the integral in Eq. (96) shows that the critical temperature vanishes logarithmically

$$\theta_c(\alpha) \underset{\alpha \rightarrow 2^-}{\sim} \frac{1}{|\ln(2-\alpha)|}. \quad (97)$$

The full phase diagram in the (α, θ) plane is shown in Fig. 8, where the critical line $\theta_c(\alpha)$ separates the active and passive regimes of the RTP stationary state.

2. Universal Low-D Scaling Form Around $z = \pm \frac{v_0}{\mu}$

As discussed in the previous section, in the vanishing noise limit $D \rightarrow 0$, the stationary density $p_Z(z)$ exhibits algebraic singularities at the turning points $z = \pm v_0/\mu$ for $\alpha < 2$. For finite $D > 0$, the thermal fluctuations regularize these divergences and allow the particle to perform excursions beyond the $D = 0$ finite support $[-v_0/\mu, v_0/\mu]$. This smoothening mechanism manifests itself in the emergence of a boundary layer of width $\mathcal{O}(\sqrt{D})$ around the turning points. To characterize the behavior of the distribution in this regime, we focus on the right turning point $\tilde{z} = 1$ (corresponding to $z = v_0/\mu$). The analysis for the left turning point follows by symmetry. We introduce the scaling variable $\lambda = (\tilde{z} - 1)/\sqrt{\theta}$, where θ is given in Eq. (92), to describe the vicinity of the turning point. By analyzing the integral representation in Eq. (91) in the scaling limit $\theta \rightarrow 0$, $\tilde{z} \rightarrow 1$ with λ fixed, we obtain the following scaling form

$$f_\theta(\tilde{z}) \sim \theta^{\frac{\alpha}{4} - \frac{1}{2}} F_\alpha \left(\lambda = \frac{\tilde{z} - 1}{\sqrt{\theta}} \right), \quad \text{where } F_\alpha(\lambda) = \frac{\Gamma(\frac{\alpha+1}{2})}{\pi \Gamma(\frac{\alpha}{2})} 2^{\frac{\alpha}{2}-1} \int_0^{+\infty} dv e^{-(v+\lambda)^2} v^{\frac{\alpha}{2}-1}. \quad (98)$$

It is instructive to examine the asymptotic behaviors of this scaling function in the limits $\lambda \rightarrow \mp\infty$, which describe the matching with the bulk and the tail of the distribution respectively. A straightforward asymptotic analysis of the

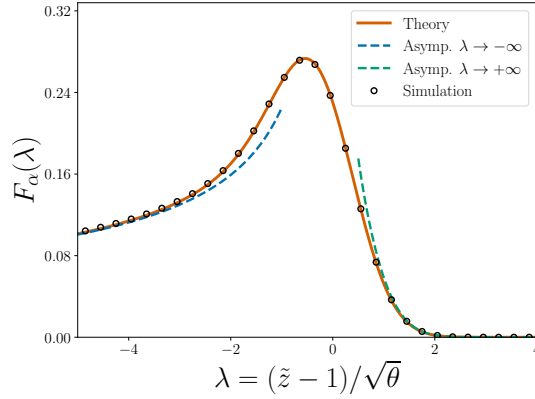


FIG. 9. Universal low- D turning-point scaling of the stationary position distribution for a one-dimensional run-and-tumble particle in a harmonic trap in the presence of thermal noise. Symbols show simulations for $\mu = 1.0$, $v_0 = 1.0$, $\alpha = \gamma/\mu = 1.0$, and $\theta = 2\mu D/v_0^2 = 10^{-4}$, plotted versus the scaled coordinate $\lambda = (\tilde{z} - 1)/\sqrt{\theta}$ with $\tilde{z} = \mu z/v_0$. The solid curve is the theoretical scaling function $F_\alpha(\lambda)$ from Eq. (98), while the dashed curves show the asymptotic forms in Eq. (99) for $\lambda \rightarrow -\infty$ (interior matching) and $\lambda \rightarrow +\infty$ (exterior tail).

integral representation of $F_\alpha(\lambda)$ in Eq. (98) yields

$$F_\alpha(\lambda) \sim \begin{cases} \frac{\Gamma(\frac{\alpha+1}{2})}{\sqrt{\pi} \Gamma(\frac{\alpha}{2})} 2^{\frac{\alpha}{2}-1} |\lambda|^{\frac{\alpha}{2}-1}, & \text{as } \lambda \rightarrow -\infty, \\ \frac{\Gamma(\frac{\alpha+1}{2})}{2\pi} \lambda^{-\frac{\alpha}{2}} e^{-\lambda^2}, & \text{as } \lambda \rightarrow +\infty. \end{cases} \quad (99)$$

These limits ensure a smooth crossover between the different regimes of the density. For $\lambda \rightarrow -\infty$ (corresponding to the interior of the active domain), substituting the asymptotic form back into Eq. (98) recovers the algebraic divergence of the $D = 0$ RTP distribution $p_X(x)$ near the edge, as given in Eq. (59). Conversely, for $\lambda \rightarrow +\infty$ (the exterior region), the decay of $F_\alpha(\lambda)$ matches the form derived in Eq. (93). In Fig. 9, we test the scaling prediction against simulations by plotting the universal function $F_\alpha(\lambda)$ from Eq. (98) together with its asymptotic forms in Eq. (99), finding a perfect agreement.

B. Stationary State of a Two-Dimensional RTP with $D > 0$

In two dimensions, the single component stationary state $p_Z(z)$ of the RTP with $D > 0$ is given by Eq. (89) where the function $p_X(x)$ is the beta function from Eq. (65). In the presence of the thermal noise, the support of $p_Z(z)$ is now extended to the whole real line $(-\infty, +\infty)$. Hence, using isotropy, the distribution of the radius can then be computed using the first line of Eq. (11), where the upper bound of the integral is instead $+\infty$. Straightforward calculations then lead to

$$p_R\left(\tilde{r} = \frac{\mu r}{v_0}\right) = \sqrt{\frac{2}{D\mu}} \frac{v_0^2}{\pi D} \frac{\Gamma(1+\alpha)}{\Gamma(\frac{1}{2}+\alpha)} \tilde{r} \int_{\tilde{r}}^{+\infty} \frac{d\tilde{z}}{\sqrt{\tilde{z}^2 - \tilde{r}^2}} \int_{-1}^1 d\tilde{x} (\tilde{z} - \tilde{x})(1 - \tilde{x}^2)^{\alpha - \frac{1}{2}} e^{-\frac{v_0^2}{2D\mu}(\tilde{x} - \tilde{z})^2}. \quad (100)$$

For a comparison with simulation, see the middle panel of Fig. 7. From the radial distribution, we find that the joint distribution in $d = 2$ is given by

$$P(x, y) = \frac{p_R\left(r = \sqrt{x^2 + y^2}\right)}{2\pi r} = \left(\frac{\mu}{v_0}\right)^2 g_\theta\left(\tilde{r} = \frac{\mu r}{v_0}\right), \quad (101)$$

$$g_\theta(\tilde{r}) = \frac{2}{\pi^2} \frac{1}{\theta^{\frac{3}{2}}} \frac{\Gamma(1+\alpha)}{\Gamma(\frac{1}{2}+\alpha)} \int_{\tilde{r}}^{+\infty} d\tilde{z} \int_{-1}^1 d\tilde{x} \frac{(\tilde{z} - \tilde{x})}{\sqrt{\tilde{z}^2 - \tilde{r}^2}} (1 - \tilde{x}^2)^{\alpha - \frac{1}{2}} e^{-\frac{(\tilde{x} - \tilde{z})^2}{\theta}}. \quad (102)$$

In the right panel of Fig. 8 we show a 3D plot of $P(x, y)$ as a function of (x, y) for two different sets of parameters. In the top-right (for high- D or equivalently high- θ), $P(x, y)$ has a bell shape with a unique maximum at the origin

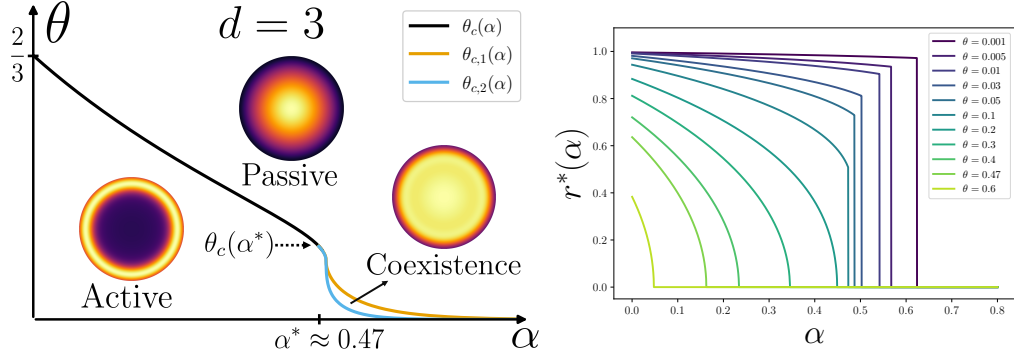


FIG. 10. **Left:** The three plots are cross sections $P(x, y, 0)$ as a function of (x, y) calculated using Eq. (105) illustrating the finite- D shape transition in $d = 3$. The black curve shows the analytic critical line obtained from Eq. (107): it exists only up to the value $\alpha^* \simeq 0.47$ (i.e., there is no solution to this equation for $\alpha > \alpha^*$). For $\alpha \leq \alpha^*$, this line separates a phase with a single maximum at the origin from a phase where the origin becomes a local minimum and a shell-like maximum develops near the turning sphere $r \simeq v_0/\mu$. For $\alpha > \alpha^*$, the transition occurs instead in two steps and across two critical lines computed numerically. The upper line $\theta_{c,1}(\alpha)$ (orange) marks the emergence of an outer local maximum while the origin remains the global maximum. The lower line $\theta_{c,2}(\alpha)$ (blue) corresponds to an abrupt change of the location of the global maximum from the origin to the outer shell. In the intermediate region $\theta_{c,2}(\alpha) < \theta < \theta_{c,1}(\alpha)$, $P(x, y, z)$ is nearly flat for $r \in [0, v_0/\mu]$ and exhibits two maxima (a global one at the origin and a local one at $r \simeq v_0/\mu$). **Right:** For several fixed values of θ , we show the numerically evaluated position of the global maximum $r^*(\alpha)$ of $h(r)$ given in Eq. (105). For $\theta > \theta_c(\alpha^*) \approx 0.47 \simeq 0.15$, $r^*(\alpha)$ moves continuously from the origin to the turning sphere of radius $r_0 = v_0/\mu$ as α is varied. In contrast, for $\theta < \theta_c(\alpha^*)$, $r^*(\alpha)$ exhibits an abrupt jump between $r = 0$ and $r \simeq v_0/\mu$ upon crossing $\theta_{c,2}(\alpha)$.

$(x = 0, y = 0)$ while in the bottom left (for low- D or equivalently low- θ) the origin is a local minimum with a local maximum on a ring of radius $r_0 \approx v_0/\mu$. This is a manifestation of the shape transition, similar to the one found in $d = 1$, which we now describe in more detail.

As in $d = 1$, the passive to active shape transition is characterized by the value of θ at which the maximum of $P(x, y)$ at the origin becomes a local minimum. Equivalently, the critical line $\theta_c(\alpha)$ is determined by the condition $g_\theta''(\tilde{r} = 0) = 0$. Using the change of variables $u = \sqrt{\tilde{z}^2 - \tilde{r}^2}$, one finds that the resulting equation that determines $\theta_c(\alpha)$ can be written, for $\alpha < 1$, as

$$\int_0^{+\infty} du \int_0^1 dx (1 - x^2)^{\alpha - \frac{1}{2}} \left[\frac{x}{2u^3} \left(e^{-\frac{(u-x)^2}{\theta_c(\alpha)}} - e^{-\frac{(u+x)^2}{\theta_c(\alpha)}} \right) - \frac{1}{u^2 \theta_c(\alpha)} \left((u-x)^2 e^{-\frac{(u-x)^2}{\theta_c(\alpha)}} + (u+x)^2 e^{-\frac{(u+x)^2}{\theta_c(\alpha)}} \right) \right] = 0. \quad (103)$$

By solving numerically this equation for $\theta_c(\alpha)$ one finds the black solid line shown in Fig. 8, which separates the passive and active in the (α, θ) plane. One can numerically check that $\theta_c(\alpha) \rightarrow 1$ when $\alpha \rightarrow 0$ and $\theta_c(\alpha) \rightarrow 0$ when $\alpha \rightarrow 1$ – see Fig. 8.

C. Stationary State of a Three-Dimensional RTP with $D > 0$

In the three dimensional case, the expressions are more involved. One has to inject the formula at zero temperature given in Eq. (70) inside Eq. (89) to obtain the single component distribution with $D > 0$. That is,

$$p_Z(z) = \frac{\alpha e^\alpha}{2\pi} \frac{\mu}{v_0} \sqrt{\frac{\mu}{2\pi D}} \int_{-\frac{v_0}{\mu}}^{\frac{v_0}{\mu}} dx e^{-\frac{\mu(z-x)^2}{2D}} \int_0^{\frac{1}{2}(1+\frac{\mu x}{v_0})} du \left[\frac{1}{2} \left(1 + \frac{\mu x}{v_0} \right) - u \right]^{\alpha-1} f(u), \quad (104)$$

where $f(u)$ is the function given in Eq. (71). Then, when $d = 3$, one finally has to compute $p_R(r) = -2rp'_Z(r)$ to obtain the radial distribution. We check that the result agrees with simulations in the right panel of Fig. 7. The joint law is then given by

$$P(x, y, z) = h\left(r = \sqrt{x^2 + y^2 + z^2}\right) = \frac{p_R(r)}{4\pi r^2} = -\frac{p'_Z(r)}{2\pi r}. \quad (105)$$

A plot of $P(x, y, z = 0)$ as a function of (x, y) is shown in the left panel of Fig. 10 for different values of the parameters. For small values of $\alpha < \alpha^*$ (to be discussed below), we find a shape transition that is very similar to the one found in

$d = 1$ and $d = 2$. As above, the transition occurs when the maximum at the origin becomes a local minimum. It is therefore given by the condition $h''(r) = 0$ which here is equivalent to $p_Z^{(4)}(r) = 0$ (since $p'_Z(z = 0) = 0$ by symmetry). Using the change of variables $\tilde{x} = \mu x/v_0$ and $\tilde{z} = \mu z/v_0$ as well as the identity

$$\frac{\partial^4}{\partial \tilde{z}^4} e^{-\frac{(\tilde{z}-\tilde{x})^2}{\theta}} \Big|_{z=0} = \frac{4}{\theta^2} (3\theta^2 - 12\theta\tilde{x}^2 + 4\tilde{x}^4) e^{-\frac{\tilde{x}^2}{\theta}}, \quad (106)$$

one finds that the condition in $d = 3$ reads

$$\int_{-1}^1 d\tilde{x} (3\theta_c(\alpha)^2 - 12\theta_c(\alpha)\tilde{x}^2 + 4\tilde{x}^4) e^{-\frac{\tilde{x}^2}{\theta_c(\alpha)}} \int_0^{\frac{1}{2}(1+\tilde{x})} du \left[\frac{1}{2}(1+\tilde{x}) - u \right]^{\alpha-1} f(u) = 0. \quad (107)$$

Numerically, we find that Eq. (107) admits a unique solution only up to the value $\alpha^* \simeq 0.47$ – see the left panel of Fig. 10. Hence, for $\alpha < \alpha^*$, the behavior remains analogous to $d = 1, 2$, and Eq. (107) yields a single critical line separating a phase with a unique maximum at $r = 0$ from a phase where the origin becomes a local minimum when a maximum of $P(x, y, z)$ develops on a shell near the “turning sphere” $r \simeq v_0/\mu$.

Interestingly, Eq. (107) can be studied analytically in the limit $\alpha \rightarrow 0$ as follows. Using the $\alpha \rightarrow 0$ asymptotics of p_X in Eq. (50), we find in $d = 3$

$$p_X(x) \xrightarrow{\alpha \rightarrow 0} \mu W(\mu x) = \frac{\mu}{2v_0}, \quad (108)$$

since $W(v) = 1/(2v_0)$ on $[-v_0, v_0]$. Substituting this limiting form into the convolution formula Eq. (89) yields an explicit expression for p_Z . Imposing the transition criterion $p_Z^{(4)}(0) = 0$ then gives

$$\theta_c(\alpha \rightarrow 0) = \frac{2}{3}. \quad (109)$$

For $\alpha > \alpha^*$, Eq. (107) has no solution, and, for fixed $\alpha > \alpha^*$ the shape transition occurs instead in two steps as θ crosses the two distinct lines $\theta_{c,1}(\alpha)$ and $\theta_{c,2}(\alpha) < \theta_{c,1}(\alpha)$ in the (α, θ) plane – see Fig. 10. These two lines are found by numerically identifying the location of the maxima of $P(x, y, z)$ given in Eq. (105). For $\theta > \theta_{c,1}(\alpha)$ the distribution has a single maximum at the origin. For $\theta_{c,2}(\alpha) < \theta < \theta_{c,1}(\alpha)$, an additional outer local maximum appears near $r \simeq v_0/\mu$ while the origin remains the global maximum, leading to a broad, nearly flat profile on $r \in [0, v_0/\mu]$ with two competing maxima (see again Fig. 10, left panel). Below the lower critical line $\theta < \theta_{c,2}(\alpha)$ the global maximum of $P(x, y, z)$ is located at the outer shell near $r \simeq v_0/\mu$. Interestingly, as θ crosses the lower critical line $\theta = \theta_{c,2}(\alpha)$ the location of the global maximum jumps (discontinuously) from the origin to the outer shell, similar to a first-order transition. This two-step transition can also be probed by varying α , for a fixed value of θ . In this case, for sufficiently small value of θ , the location of the global maximum $r^*(\alpha)$ jumps discontinuously from a finite value $r^*(\alpha) > 0$ to $r^*(\alpha) = 0$ as α increases and crosses some critical value, as shown in the right panel of Fig. 10.

VI. STATIONARY DISTRIBUTION OF A N -STATE RTP

Up to now, we have only considered the case where $W(v)$ is a continuous distribution. However, in many cases, it is relevant to consider a case where the velocities can only take discrete values. This amounts to consider a N -state model where $W(v)$ is given by

$$W(v) = \sum_{i=1}^N p_i \delta(v - v_i), \quad 0 < p_i < 1, \quad \sum_{i=1}^N p_i = 1. \quad (110)$$

Without loss of generality, we assume the velocities to be ordered: $v_1 < \dots < v_N$. As mentioned above, the one dimensional RTP corresponds to a two-state process with velocities $\pm v_0$ and probabilities $p_1 = p_2 = 1/2$. Different extensions, including RTP models with multiple internal velocity states have also been considered. For instance, three-state [72, 86] and four-state [42] cases have been investigated. In both cases, the stationary distributions were obtained by solving coupled Fokker-Planck equations, which quickly becomes a hard task as N increases. Here, using the Dirichlet-process (stick-breaking) representation and the general formula (16) obtained in this paper, we obtain the stationary state for an arbitrary N -state RTP in a direct and systematic way.

Cifarelli-Regazzini Representation. The stationary state can be obtained from Eq. (45). For the N -state distribution (110), one first shows that

$$\phi_\alpha(t) = \sin\left(\pi\alpha \sum_{i=1}^k p_i \Theta\left(t - \frac{v_i}{\mu}\right)\right) \prod_{i=1}^N |t - v_i/\mu|^{-\alpha p_i}. \quad (111)$$

To avoid the appearance of delta-function terms in Eq. (16) when deriving the Heaviside functions in (111), one can consider the calculation of the derivative of $\phi_\alpha(t)$ for values $t \neq v_i/\mu$. One finds

$$\frac{d\phi_\alpha(t)}{dt} = -\alpha \phi_\alpha(t) \sum_{i=1}^N \frac{p_i}{t - v_i/\mu}. \quad (112)$$

Then, using (112), we find that the stationary density (16) is piecewise continuous on the intervals $x \in]v_k/\mu, v_{k+1}/\mu[$, and its explicit form is

$$\begin{aligned} p_X(x) = & -\frac{\alpha}{\pi} \left[\sum_{m=1}^{k-1} \sin\left(\pi\alpha \sum_{i=1}^m p_i\right) \int_{v_m/\mu}^{v_{m+1}/\mu} dt (x-t)^{\alpha-1} \left(\sum_{i=1}^N \frac{p_i}{t - \frac{v_i}{\mu}}\right) \prod_{i=1}^N |t - v_i/\mu|^{-\alpha p_i} \right. \\ & \left. + \sin\left(\pi\alpha \sum_{i=1}^k p_i\right) \int_{v_k/\mu}^x dt (x-t)^{\alpha-1} \left(\sum_{i=1}^N \frac{p_i}{t - \frac{v_i}{\mu}}\right) \prod_{i=1}^N |t - v_i/\mu|^{-\alpha p_i} \right]. \end{aligned} \quad (113)$$

The case $\alpha = 1$. In that case, we can directly use the general expression (48). It yields

$$p_X(x) = \frac{\phi_1(x)}{\pi} = \frac{1}{\pi} \sin\left(\pi \sum_{i=1}^k p_i\right) \prod_{i=1}^N |x - v_i/\mu|^{-p_i}, \quad x \in]v_k/\mu, v_{k+1}/\mu[. \quad (114)$$

Dirichlet Representation. Another explicit formula for the stationary state can be found from the result (43) which gives the stationary position of the generalized RTP in terms of stick-breaking weights. In the case of this N -state model, for a given trajectory and a given sequence of velocities $\{v_1, \dots, v_n\}$, distinct samples v_i drawn from $W(v)$ may take identical values v_j . Hence, one must aggregate the corresponding weights in the equation (43), leading to

$$X = \frac{1}{\mu} \sum_{n \geq 1} v_n Y_n = \frac{1}{\mu} \sum_{n=1}^N v_n Z_n, \quad Z_n = \sum_{i \geq 1} Y_i \mathbf{1}_{v_i=v_n}. \quad (115)$$

It is known that these aggregated weights Z_n follow a Dirichlet distribution [75, 76]

$$(Z_1, \dots, Z_N) \stackrel{d}{=} \text{Dir}(\alpha p_1, \dots, \alpha p_N), \quad (116)$$

where $\text{Dir}(\cdot)$ denotes the Dirichlet distribution. The corresponding joint probability density reads

$$f_{\text{Dir}}(z_1, \dots, z_N) = \frac{\Gamma(\alpha)}{\prod_{i=1}^N \Gamma(\alpha p_i)} \left(\prod_{i=1}^N z_i^{\alpha p_i - 1} \right) \delta\left(1 - \sum_{i=1}^N z_i\right) \mathbf{1}_{\{z_i \geq 0\}}, \quad (117)$$

and since the position of the RTP is $X = \frac{1}{\mu} \sum_{n=1}^N v_n Z_n$, its probability density can be expressed as

$$p_X(x) = \left\langle \delta\left(x - \frac{1}{\mu} \sum_{n=1}^N v_n z_n\right) \right\rangle_z \quad (118)$$

$$= \frac{\Gamma(\alpha)}{\prod_{i=1}^N \Gamma(\alpha p_i)} \int_0^1 dz_1 \cdots \int_0^1 dz_N \delta\left(x - \frac{1}{\mu} \sum_{n=1}^N v_n z_n\right) \left(\prod_{i=1}^N z_i^{\alpha p_i - 1} \right) \delta\left(1 - \sum_{i=1}^N z_i\right). \quad (119)$$

Note that this result can also be derived directly from the expression of the MGF given in Eq. (36). In Appendix E, we compute the stationary state of a general 3-state RTP and compare our theoretical predictions to simulation results. We finally mention that these results can be straightforwardly generalized in the presence of an additional thermal noise using the convolution structure in Eq. (89).

VII. CONCLUSION

In this work, we have obtained the exact nonequilibrium stationary state distribution of a run-and-tumble particle confined by an isotropic harmonic potential in arbitrary spatial dimension d , including a closed-form characterization in $d = 3$. Exploiting rotational invariance, we showed that the full stationary distribution is determined by a single Cartesian marginal $p_X(x)$: the radial distribution $p_R(r)$ and the joint density $P(x_1, \dots, x_d)$ follow from $p_X(x)$ through explicit projection/inversion transforms. Our central analytical result is an exact solution of a generalized one-dimensional RTP in a harmonic trap where post-tumble velocities are sampled from an arbitrary law $W(v)$. Obtaining the stationary solution via the standard Fokker–Planck approach leads to a nonlocal integro-differential equation that does not appear analytically tractable. Although this route proves unproductive, the problem can be solved by a completely different approach. In particular, the position in the stationary state yields a Kesten recursion relation. Solving it explicitly shows that the position of this generalized RTP in the stationary state identifies with a mean functional of a Dirichlet process via a stick-breaking construction. This connection to Dirichlet processes allowed us to obtain closed-form expressions for $p_X(x)$ and for its stationary moments, for an arbitrary law $W(v)$. Specializing $W(v)$ to the projected velocity distribution of an isotropic RTP then provides the complete stationary statistics of an RTP in a harmonic well in any dimension d .

A key physical scale of the dynamics is the turning radius $r_0 = v_0/\mu$, where self-propulsion velocity v_0 and harmonic restoring force of strength μ balance. Varying the dimensionless activity parameter $\alpha = \gamma/\mu$, where γ is the tumbling rate, controls the shape of the stationary distribution around this turning surface. In $d = 1$ and $d = 2$, the radial law reduces to a beta distribution and develops integrable edge singularities in the persistent regime, with accumulation near r_0 . In $d = 3$, we have shown that the stationary distribution remains explicitly computable but no longer collapses to a beta distribution. The stationary distribution $p_R(r)$ of the radius of the position, both in $d = 2$ and $d = 3$, exhibits a shape transition at $\alpha = 1$: we find that $p_R(r)$ diverges as $r \rightarrow r_0$ for $\alpha < 1$ while $p_R(r) \rightarrow 0$ as $r \rightarrow r_0$ for $\alpha > 1$.

We have also studied the effects of thermal fluctuations by adding a Gaussian white noise of diffusivity $D > 0$. For an RTP in a harmonic well, it turns out that the stationary state for $D > 0$ is a Gaussian convolution of the $D = 0$ stationary state. This provides an exact description of how temperature rounds off turning-point singularities and extends the support of the stationary distribution of the position beyond r_0 . This representation reveals a crossover between persistence-dominated and diffusion-dominated regimes and yields universal low- D scaling forms near the turning surface. In $d = 1$ and $d = 2$, lowering D at fixed activity produces a clear unimodal-to-bimodal crossover of the stationary density, with two maxima that approach the turning points as $D \rightarrow 0$. In $d = 3$, the same trend holds up to a critical value of α , beyond which two peaks coexist and the global maximum jumps discontinuously from the origin to the outer shell at $r = r_0$.

Throughout the paper, we have assumed a constant run speed v_0 in $d > 1$ (see Eq. (2)). It would be interesting to extend this framework if one allows v_0 to be drawn from a prescribed distribution, which modifies the projected component of the velocity. Importantly, Eq. (16) remains unchanged. This extension is particularly relevant for experimental systems, such as bacteria exhibiting run-and-tumble motion, in which run speeds are indeed heterogeneous [90, 91].

Starting from the exact stationary state obtained via the Dirichlet-process (stick-breaking) representation, several extensions are natural. One is to relax rotational invariance and study anisotropic confinement, for instance, quadratic traps of the form $V(\mathbf{r}) = \frac{1}{2} \sum_{i=1}^d \mu_i x_i^2$ with different μ_i 's. In this setting, the stationary distribution (and moments) of each Cartesian component can be obtained exactly using Eq. (16). Although reconstructing the full radial distribution from these marginals is nontrivial, the isotropic stationary distribution $p_R(r)$ derived in this paper still provides a convenient baseline for perturbative treatments of the corresponding Fokker-Planck equation around the isotropic limit.

Finally, we expect the analytical techniques developed here to be relevant to study other types of switching dynamics, which have generated some recent interest. A notable example is switching diffusion, i.e., Brownian motion with a diffusivity that changes randomly in time according to a prescribed law [86, 92]. More broadly, the same approach should apply to linear Langevin dynamics in switching environments, including many-particle systems undergoing Brownian motion in a harmonic potential whose stiffness switches in time [89, 93, 94]. In such cases, the switching dynamics of the trap induces dynamical emergent correlations between the particles and it will be interesting to

extend the techniques used here to such many-body correlated systems.

Acknowledgments. We acknowledge support from ANR Grant No. ANR-23-CE30-0020-01 EDIPS. MG is grateful to Christina Kurzthaler for many interesting discussions on related problems.

APPENDICES

Appendix A: Identities and Isotropy-Based Derivations

1. Derivation of $W_{\text{proj}}(v)$

In this appendix, for the sake of completeness, we provide a derivation of the projected velocity law of an isotropic RTP $W_{\text{proj}}(v)$ given in Eq. (7). This derivation can also be found in Ref. [50]. Consider a random unit vector $\mathbf{n} = (n_1, n_2, \dots, n_d) \in \mathbb{R}^d$ drawn uniformly from the unit sphere S^{d-1} , and we assume $d \geq 2$. During a run, the particle governed by the Langevin dynamics in Eq. (2) experiences the active force $\mathbf{v} = v_0 \mathbf{n}$. Due to isotropy, all components are statistically equivalent. Without loss of generality, we therefore focus on the first component, i.e., the scalar projection $v_1 = v_0 n_1$. We want to compute its PDF which we denote as $W_{\text{proj}}(v)$. The PDF of \mathbf{v} with length v_0 is simply given by

$$P(\mathbf{v}) = \frac{1}{\Omega_{d-1} v_0^{d-1}} \delta(|\mathbf{v}| - v_0), \quad \Omega_{d-1} = \frac{2\pi^{d/2}}{\Gamma(d/2)}, \quad (\text{A1})$$

where Ω_{d-1} is the surface area of the unit sphere S^{d-1} . Using the standard identity for the Dirac delta under a change of variables, $\delta(|\mathbf{v}| - v_0) = 2v_0 \delta(|\mathbf{v}|^2 - v_0^2)$, we can equivalently rewrite the density in terms of $|\mathbf{v}|^2$, which will be convenient when integrating out components:

$$P(\mathbf{v}) = \frac{2}{\Omega_{d-1} v_0^{d-2}} \delta(|\mathbf{v}|^2 - v_0^2), \quad |\mathbf{v}|^2 = v_1^2 + v_2^2 + \dots + v_d^2, \quad (\text{A2})$$

where $v_i = v_0 n_i$. We now compute the marginal distribution of v_1 by integrating over the remaining components. Introducing a delta constraint $\delta(v_1 - v)$ to fix the first component, we obtain

$$W_{\text{proj}}(v) = \int P(\mathbf{v}) \delta(v_1 - v) dv_1 dv_2 \dots dv_d = \frac{2}{\Omega_{d-1} v_0^{d-2}} \int \delta(|\mathbf{v}|^2 - v_0^2) dv_2 dv_3 \dots dv_d. \quad (\text{A3})$$

To evaluate the remaining integral, we switch to hyperspherical coordinates in the $(d-1)$ -dimensional subspace spanned by (v_2, \dots, v_d) . Let $\rho^2 = v_2^2 + \dots + v_d^2$ so that the $(d-1)$ -dimensional volume element becomes $dv_2 \dots dv_d = \Omega_{d-2} \rho^{d-2} d\rho$. With this substitution the marginal reduces to

$$W_{\text{proj}}(v) = \frac{2\Omega_{d-2}}{\Omega_{d-1} v_0^{d-2}} \int_0^{+\infty} \delta(\rho^2 - (v_0^2 - v^2)) \rho^{d-2} d\rho. \quad (\text{A4})$$

Next, we set $u = \rho^2$, so that $du = 2\rho d\rho$ and hence

$$W_{\text{proj}}(v) = \frac{\Omega_{d-2}}{\Omega_{d-1} v_0^{d-2}} \int_0^{+\infty} \delta(u - (v_0^2 - v^2)) u^{\frac{d-3}{2}} du. \quad (\text{A5})$$

Performing the integration and simplifying the prefactor, we obtain the result given in the main text

$$W_{\text{proj}}(v) = \frac{1}{v_0} \frac{\Gamma(\frac{d}{2})}{\sqrt{\pi} \Gamma(\frac{d-1}{2})} \left(1 - \frac{v^2}{v_0^2}\right)^{\frac{d-3}{2}}, \quad -v_0 \leq v \leq v_0. \quad (\text{A6})$$

2. Identities Between $p_X(x)$ and $p_R(r)$

As the motion is isotropic, all components of the d -dimensional position x_i 's are identically distributed. Focusing on the first component $x \equiv x_1$, we have

$$X = R n_1, \quad (\text{A7})$$

where n_1 is the first component of a random unit vector $\mathbf{n} = (n_1, n_2, \dots, n_d) \in \mathbb{R}^d$ drawn uniformly from the unit sphere S^{d-1} ($d \geq 2$). From the above derivation of $W_{\text{proj}}(v)$ in Eq. (A6), it follows that the conditional density of $X = x$ at fixed radius $R = r$ is given by the same projection law with the replacement $v_0 \rightarrow r$, namely

$$p(x|r) = \frac{1}{r} \frac{\Gamma(\frac{d}{2})}{\sqrt{\pi} \Gamma(\frac{d-1}{2})} \left(1 - \frac{x^2}{r^2}\right)^{\frac{d-3}{2}}, \quad -r \leq x \leq r. \quad (\text{A8})$$

Averaging over R , whose PDF $p_R(r)$ is supported on $0 \leq r \leq v_0/\mu$, we obtain the marginal PDF of x (see also [52])

$$p_X(x) = \frac{\Gamma(\frac{d}{2})}{\sqrt{\pi} \Gamma(\frac{d-1}{2})} \int_{|x|}^{v_0/\mu} dr \frac{p_R(r)}{r} \left(1 - \frac{x^2}{r^2}\right)^{\frac{d-3}{2}}. \quad (\text{A9})$$

In particular, $p(x) = 0$ for $|x| > v_0/\mu$. We are now interested in inverting Eq. (A9) in $d = 2$, and $d = 3$, to obtain a relation for $p_R(r)$ given $p_X(x)$.

Inversion in $d = 2$. Let us focus on the case $x > 0$ (this is sufficient since $p_X(x)$ is symmetric). We have

$$p_X(x) = \frac{1}{\pi} \int_x^{v_0/\mu} dr \frac{p_R(r)}{\sqrt{r^2 - x^2}}. \quad (\text{A10})$$

Now introduce $u = x^2$, $v = r^2$, $u^* = (v_0/\mu)^2$, and the functions

$$g(u) = \pi p_X(\sqrt{u}), \quad f(v) = \frac{p_R(\sqrt{v})}{2\sqrt{v}}, \quad (\text{A11})$$

so that

$$g(u) = \int_u^{u^*} dv \frac{f(v)}{\sqrt{v-u}}, \quad 0 \leq u \leq u^*. \quad (\text{A12})$$

Define

$$I(s) := \int_s^{u^*} du \frac{g(u)}{\sqrt{u-s}} = \int_s^{u^*} du \frac{1}{\sqrt{u-s}} \left(\int_u^{u^*} \frac{f(v)}{\sqrt{v-u}} dv \right), \quad 0 \leq s \leq u^*. \quad (\text{A13})$$

On the integration domain we have $s \leq u \leq v \leq u^*$. Swapping the order of integration yields

$$I(s) = \int_s^{u^*} f(v) \underbrace{\left(\int_s^v \frac{du}{\sqrt{(u-s)(v-u)}} \right)}_{=\pi} dv. \quad (\text{A14})$$

Hence, we obtain

$$I'(s) = -\pi f(s) \implies f(s) = -\frac{1}{\pi} \frac{d}{ds} \left(\int_s^{u^*} du \frac{g(u)}{\sqrt{u-s}} \right). \quad (\text{A15})$$

Performing the change of variable $u = s + t^2$, and applying Leibniz's rule for differentiation under the integral sign yields

$$f(s) = -\frac{1}{\pi} \int_s^{u^*} du \frac{g'(u)}{\sqrt{u-s}}, \quad 0 \leq s \leq u^*. \quad (\text{A16})$$

Reverting to the original variables, we thus arrive at the result (11) reported in the main text

$$p_R(r) = -2r \int_r^{v_0/\mu} dx \frac{p'_X(x)}{\sqrt{x^2 - r^2}}, \quad 0 \leq r \leq v_0/\mu. \quad (\text{A17})$$

Inversion in $d = 3$. In this case, the calculation is straightforward. Setting $d = 3$ in Eq. (A9) gives

$$p_X(x) = \frac{1}{2} \int_{|x|}^{v_0/\mu} dr \frac{p_R(r)}{r}. \quad (\text{A18})$$

Differentiating with respect to x then yields the inversion formula given in (11), i.e.,

$$p_R(r) = -2r p'_X(r). \quad (\text{A19})$$

3. Moments

From Eq. (A7), $X = R n_1$, and using that the radial variable R and the uniform orientation \mathbf{n} are independent, the moments factorize as

$$\langle |X|^n \rangle = \langle R^n \rangle \langle |n_1|^n \rangle, \quad \langle |n_1|^n \rangle = \frac{\Gamma(\frac{d}{2}) \Gamma(\frac{n+1}{2})}{\Gamma(\frac{1}{2}) \Gamma(\frac{n+d}{2})}. \quad (\text{A20})$$

Here, $\langle |n_1|^n \rangle$ is the n -th moment of the projection law W_{proj} in Eq. (A6) evaluated at $v_0 = 1$. Eliminating $\langle |n_1|^n \rangle$ in Eq. (A20) yields

$$\langle R^n \rangle = \frac{\Gamma(\frac{1}{2}) \Gamma(\frac{n+d}{2})}{\Gamma(\frac{d}{2}) \Gamma(\frac{n+1}{2})} \langle |X|^n \rangle. \quad (\text{A21})$$

The even moments of R follow directly from the moments of X given in Eq. (47):

$$\langle R^{2n} \rangle = \frac{\Gamma(\frac{1}{2}) \Gamma(n + \frac{d}{2})}{\Gamma(\frac{d}{2}) \Gamma(n + \frac{1}{2})} \langle X^{2n} \rangle. \quad (\text{A22})$$

4. Relation Between the Joint Law and the Radial Law

Using the invariance of the system under rotation, the joint density of an RTP in d dimensions depends only on the radius $r = \sqrt{x_1^2 + \dots + x_d^2}$, so there exists a function f_R such that

$$P(x_1, \dots, x_d) = f_R\left(r = \sqrt{x_1^2 + \dots + x_d^2}\right). \quad (\text{A23})$$

Let $R = \|X\|$ denote the radial component and let $p_R(r)$ be its density. Using spherical coordinates, we have

$$\mathbb{P}(R < r) = \int_{\|x\| < r} P(x) d^d x = \int_0^r \int_{S^{d-1}} f_R(\rho) \rho^{d-1} d\rho d\Omega_{d-1} = \Omega_{d-1} \int_0^r f_R(\rho) \rho^{d-1} d\rho,$$

where Ω_{d-1} is the surface area of the unit sphere in \mathbb{R}^d . Differentiating with respect to r yields

$$f_R(r) = \frac{p_R(r)}{\Omega_{d-1} r^{d-1}}, \quad (\text{A24})$$

which is exactly relation (12) in the main text.

Appendix B: Moment Generating Function of the Generalized RTP

1. Kesten Approach

In Section III A, we derived an integral equation satisfied by the stationary state distribution via the Kesten relation (27). We recall it here (see Eq. (34)):

$$p_X(x) = \int dU \int dV \int dx' \alpha U^{\alpha-1} \frac{\mu}{1-U} W\left(\frac{\mu V}{1-U}\right) p_X(x') \delta(x - U x' - V). \quad (\text{B1})$$

We also recall that $U \in [0, 1]$ and $V \in [(1-U)v_{\min}/\mu, (1-U)v_{\max}/\mu]$. We introduce the moment generating function (MGF) as the bilateral Laplace transform (BLT) of the stationary state of the RTP, i.e.,

$$\tilde{p}_X(q) = \langle e^{qx} \rangle = \int_{-\infty}^{+\infty} dx e^{qx} p_X(x). \quad (\text{B2})$$

Taking the BLT of Eq. (B1) yields

$$\tilde{p}_X(q) = \int dU \int dV \int dx' \alpha U^{\alpha-1} \frac{\mu}{1-U} W\left(\frac{\mu V}{1-U}\right) p_X(x') e^{q(Ux'+V)}. \quad (\text{B3})$$

Performing the integral over the variable x' leads to

$$\tilde{p}_X(q) = \int dU \int dV \alpha U^{\alpha-1} \frac{\mu}{1-U} W\left(\frac{\mu V}{1-U}\right) \tilde{p}_X(qU) e^{qV}. \quad (\text{B4})$$

Next, integrating over V gives

$$\tilde{p}_X(q) = \int_0^1 dU \alpha U^{\alpha-1} \tilde{W}\left(\frac{1-U}{\mu}q\right) \tilde{p}_X(qU). \quad (\text{B5})$$

The change of variable $\bar{q} = qU$ allows for further analytical progress. We have

$$q [q^{\alpha-1} \tilde{p}_X(q)] = \alpha \int_0^q d\bar{q} [\bar{q}^{\alpha-1} \tilde{p}_X(\bar{q})] \tilde{W}\left(\frac{q-\bar{q}}{\mu}\right). \quad (\text{B6})$$

Introducing the function $f_\alpha(q) = q^{\alpha-1} \tilde{p}_X(q)$ and the Laplace transform

$$\hat{f}_\alpha(s) = \mathcal{L}_{q \rightarrow s} [f_\alpha(q)] = \int_0^{+\infty} dq e^{-sq} f(q), \quad (\text{B7})$$

and taking the Laplace transform of Eq. (B6) – using the property $\mathcal{L}_{q \rightarrow s} [q f_\alpha(q)] = -\hat{f}'_\alpha(s)$ – we find

$$\hat{f}'_\alpha(s) = -\alpha \mu \hat{f}_\alpha(s) \hat{W}(\mu s). \quad (\text{B8})$$

Solving this differential equation yields

$$\tilde{p}_X(q) \propto q^{1-\alpha} \mathcal{L}_{s \rightarrow q}^{-1} \left[\exp\left(-\alpha \mu \int_0^s du \hat{W}(\mu u)\right) \right], \quad (\text{B9})$$

where \mathcal{L}^{-1} denotes the inverse Laplace transform. The multiplicative factor is finally determined by the normalization condition $\tilde{p}_X(0) = 1$ and is given by $\Gamma(\alpha)$. The solution (B9) was first derived in Ref. [86]. Finally, the argument of the exponential can be rewritten as

$$\int_0^s du \hat{W}(\mu u) = \int_0^s du \int_0^{+\infty} dq e^{-\mu u q} \int_{v_{\min}}^{v_{\max}} dv e^{qv} W(v) = \frac{1}{\mu} \int_{v_{\min}}^{v_{\max}} dv \log\left(s - \frac{v}{\mu}\right) W(v). \quad (\text{B10})$$

Hence,

$$\tilde{p}_X(q) = \Gamma(\alpha) q^{1-\alpha} \mathcal{L}_{s \rightarrow q}^{-1} \left[\exp\left(-\alpha \int_{v_{\min}}^{v_{\max}} dv \log\left(s - \frac{v}{\mu}\right) W(v)\right) \right]. \quad (\text{B11})$$

It can be straightforwardly shown that this is equivalent to

$$\tilde{p}_X(q) = \Gamma(\alpha) \int_{\Gamma_B} \frac{ds}{2\pi i} \exp\left(s - \alpha \int_{v_{\min}}^{v_{\max}} dv \log\left(s - \frac{v}{\mu}\right) W(v)\right), \quad (\text{B12})$$

where Γ_B is a Bromwich contour. From Eq. (B12), one can readily verify that $\tilde{p}_X(0) = 1$.

2. Moments in The Stationary State

To extract the expression for the moments from the integral representation of the MGF (B12), we first expand the logarithm inside the exponential. This yields

$$\tilde{p}_X(q) = \Gamma(\alpha) \int_{\Gamma_B} \frac{ds}{2\pi i} e^s s^{-\alpha} \exp\left[\alpha \sum_{n=1}^{+\infty} \frac{\langle v^n \rangle}{n} \left(\frac{q}{\mu s}\right)^n\right], \quad (\text{B13})$$

where $\langle v^n \rangle$ are the moments of $W(v)$. The exponential inside the integral is precisely the generating function of the complete Bell polynomials B_n [82]. It can therefore be rewritten as

$$\exp\left[\alpha \sum_{n=1}^{+\infty} \frac{\langle v^n \rangle}{n} \left(\frac{q}{\mu s}\right)^n\right] = \sum_{n=1}^{+\infty} \frac{q^n}{n!} \left(\frac{1}{\mu s}\right)^n B_n\left(1! \alpha \frac{\langle v \rangle}{1}, \dots, n! \alpha \frac{\langle v^n \rangle}{n}\right). \quad (\text{B14})$$

The contour integral over s can then be evaluated using the standard identity

$$\int_{\Gamma_B} \frac{ds}{2\pi i} e^s s^{-\alpha-n} = \frac{1}{\Gamma(\alpha+n)} \quad (\text{B15})$$

Finally, using the definition of the moment generating function, $\tilde{p}_X(q) = \sum_{n=1}^{+\infty} (q^n/n!) \langle X^n \rangle$, we identify the coefficients of q^n and obtain the exact expression for the moments:

$$\langle X^n \rangle = \frac{1}{\mu^n} \frac{\Gamma(\alpha)}{\Gamma(\alpha+n)} B_n \left(1! \alpha \frac{\langle v \rangle}{1}, \dots, n! \alpha \frac{\langle v^n \rangle}{n} \right), \quad (\text{B16})$$

which is the formula given in Eq. (18).

Appendix C: Dirichlet Process

We have shown in Section III B that the position in the stationary state is a random variable that can be written as follows:

$$X = \frac{1}{\mu} \sum_{n \geq 1} v_n Y_n, \quad Y_n = \left[\prod_{j < n} (1 - \bar{U}_j) \right] \bar{U}_n. \quad (\text{C1})$$

For a given trajectory of the RTP, one obtains a specific realization of the velocities $\{v_1, v_2, \dots, v_n\}$ (where v_i 's are drawn from $W(v_i)$), which can be associated with the corresponding weights $\{Y_1, Y_2, \dots, Y_n\}$ of a stick-breaking process (see Fig. 2). It is then possible to introduce the random empirical measure

$$G(v) = \sum_{n \geq 1} Y_n \delta(v - v_n) = Y_1 \delta(v - v_1) + Y_2 \delta(v - v_2) + \dots \quad (\text{C2})$$

With this definition, the position x can be expressed as the mean of v/μ with respect to $G(v)$, namely,

$$X = \int_{v_{\min}}^{v_{\max}} dv \frac{v}{\mu} G(v). \quad (\text{C3})$$

The random measure $G(v)$ is precisely a realization of a Dirichlet process with concentration parameter α and base distribution $W(v)$ [76, 77]: we denote this as $G(v) \sim \text{DP}(\alpha, W)$. Correspondingly, the position x can be interpreted as the expectation of the function v/μ with respect to this random empirical measure – that is, a linear mean functional of a Dirichlet process in the terminology of the mathematical literature [75].

In Ref. [75], Cifarelli and Regazzini have derived the cumulative distribution of a linear mean functional of a Dirichlet process (see Theorem 1 of [75]), i.e., the cumulative distribution $M(x)$ of x given in Eq. (C3). It is given by

$$M(x) = \frac{1}{\pi} \int_{v_{\min}/\mu}^x dt (x-t)^{\alpha-1} \phi_\alpha(t), \quad \phi_\alpha(t) = \sin \left(\pi \alpha \int_{v_{\min}}^{\mu t} dv W(v) \right) \exp \left(-\alpha \int_{v_{\min}}^{v_{\max}} dv \log |t - \frac{v}{\mu}| W(v) \right). \quad (\text{C4})$$

Using that $(x-t)^{\alpha-1} = -\frac{1}{\alpha} \frac{d}{dt} (x-t)^\alpha$ and integrating by parts, one can then compute $p_X(x) = M'(x)$ to obtain the stationary state distribution given in the main text in Eq. (45).

1. Cifarelli–Regazzini Identity for the MGF

An important property of the mean functional of a Dirichlet process $\text{DP}(\alpha, W)$ is given by the Cifarelli–Regazzini identity. For any $\alpha > 0$, $s > -v_{\min}/\mu$, and $W(v)$ (discrete or continuous), this identity yields the expression for the following expectation value, depending on X as defined in Eq. (C3):

$$\langle (s + X)^{-\alpha} \rangle = \exp \left(-\alpha \int_{v_{\min}}^{v_{\max}} dv \log \left(s + \frac{v}{\mu} \right) W(v) \right). \quad (\text{C5})$$

From this identity, we now derive an expression for the MGF of the stationary state of the RTP defined in Eq. (B2). Using the following identity,

$$(s + X)^{-\alpha} = \frac{1}{\Gamma(\alpha)} \int_0^\infty dq e^{-qs} q^{\alpha-1} e^{-qX}, \quad (\text{C6})$$

and taking the expectation, we obtain

$$\Gamma(\alpha) \langle (s + X)^{-\alpha} \rangle = \int_0^\infty e^{-qs} q^{\alpha-1} \tilde{p}_X(-q) dq, \quad (\text{C7})$$

where we recognize the right-hand side as the Laplace transform in s of $q^{\alpha-1} \tilde{p}_X(-q)$. Therefore, taking the inverse Laplace transform and using the Cifarelli–Regazzini identity (C5) yields

$$\tilde{p}_X(q) = \Gamma(\alpha) (-q)^{1-\alpha} \mathcal{L}_{s \rightarrow -q}^{-1} \left[\exp \left(-\alpha \int_{v_{\min}}^{v_{\max}} dv \log \left(s + \frac{v}{\mu} \right) W(v) \right) \right], \quad (\text{C8})$$

where \mathcal{L}^{-1} is the inverse Laplace transform. It is possible to show that it can be rewritten exactly as Eq. (B12) which is exactly the solution that we have found via the Kesten approach.

Appendix D: Derivation of the Beta Distribution in $d = 2$

In Section IV, we showed that the stationary distribution of a component of an RTP in two dimensions can be expressed as

$$p_X(x) = \frac{\alpha \mu}{\pi} \left(\frac{2\mu}{v_0} \right)^\alpha \int_{-\frac{v_0}{\mu}}^x dt (x-t)^{\alpha-1} \psi(t), \quad \psi(t) = \frac{\cos \left(\frac{\pi \alpha}{2} + \alpha \arcsin \frac{\mu t}{v_0} \right)}{\sqrt{v_0^2 - \mu^2 t^2}}. \quad (\text{D1})$$

It turns out that this integral over t in Eq. (D1) can be performed explicitly. To see that, we first notice that $\psi(t)$ in Eq. (D1) can be written as a hypergeometric function, namely

$$\psi(t) = \frac{\cos \left(\frac{\pi \alpha}{2} + \alpha \arcsin \frac{\mu t}{v_0} \right)}{\sqrt{v_0^2 - \mu^2 t^2}} = \frac{1}{v_0 \sqrt{2 \left(1 + \frac{\mu t}{v_0} \right)}} {}_2F_1 \left(\frac{1}{2} + \alpha, \frac{1}{2} - \alpha, 1/2; \frac{1 + \frac{\mu t}{v_0}}{2} \right), \quad (\text{D2})$$

where we recall that the hypergeometric function ${}_2F_1(a, b, c; z)$ admits the series expansion

$${}_2F_1(a, b, c; z) = \sum_{k=0}^{\infty} \frac{(a)_k (b)_k}{(c)_k} z^k, \quad (\text{D3})$$

where $(x)_n = \Gamma(x+1)/\Gamma(x-n+1)$ is the Pochhammer symbol. This can be shown by observing that $\psi(t)$ satisfies a second-order differential equation of the hypergeometric type, namely

$$(\mu^2 t^2 - v_0^2) \psi''(t) + 3\mu^2 t \psi'(t) + \mu^2 (1 - \alpha^2) \psi(t) = 0, \quad (\text{D4})$$

and eventually rewriting this equation in terms of the variable $u = (1 + \mu t/v_0)/2$.

Substituting this expression (D2) in (D1) to compute $p(x = v_0(-1 + v)/\mu)$ and performing the change of variable $t = v_0(-1 + vy)/\mu$ one finds

$$p_X(x = v_0(-1 + v)/\mu) = \frac{\alpha}{\pi} 2^{\alpha-1/2} \frac{\mu}{v_0} v^{\alpha-1/2} \int_0^1 dy (1 - y)^{\alpha-1} \frac{1}{\sqrt{y}} {}_2F_1 \left(\frac{1}{2} + \alpha, \frac{1}{2} - \alpha, \frac{1}{2}, \frac{v y}{2} \right). \quad (\text{D5})$$

We now insert the series expansion (D3) in (D5) and integrate term by term, using the identity

$$\int_0^1 dy (1 - y)^{\alpha-1} y^{k-1/2} = \frac{\Gamma(\alpha) \Gamma(1/2 + k)}{\Gamma(1/2 + \alpha + k)}. \quad (\text{D6})$$

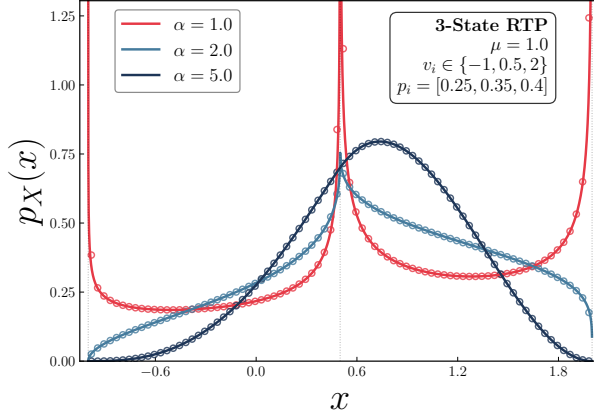


FIG. 11. Comparison of the analytical prediction Eq. (E2) for the stationary distribution of an RTP with three velocity states in a harmonic trap compared to simulation results. The solid lines represent the exact theory, while the symbols denote numerical data obtained from simulations. The distributions are shown for different values of the dimensionless switching rate $\alpha = \gamma/\mu$. Here the parameters are $\mu = 1$, $\{v_1, v_2, v_3\} = \{-1, 0.5, 2\}$, and $\{p_1, p_2, p_3\} = \{0.25, 0.35, 0.4\}$. The vertical dotted line separates the region I, for $x \in [v_1/\mu, v_2/\mu]$, from the region II for $x \in [v_2/\mu, v_3/\mu]$.

One gets, after simplification of the Pochhammer symbols and gamma functions

$$p_X(x = v_0(-1 + v)/\mu) = \frac{\alpha}{\pi} 2^{\alpha-1/2} \frac{\mu}{v_0} v^{\alpha-1/2} \sum_{k=0}^{\infty} \left(\frac{v}{2}\right)^k \frac{\cos(\alpha\pi)\Gamma(\alpha)\Gamma(1/2 - \alpha + k)}{\sqrt{\pi}\Gamma(k+1)}. \quad (\text{D7})$$

The sum over k can then be performed straightforwardly and we obtain

$$p_X(x = v_0(-1 + v)/\mu) = \frac{\alpha}{\pi^{3/2}} \frac{\mu}{v_0} \cos(\alpha\pi)\Gamma(1/2 - \alpha)\Gamma(\alpha)v^{\alpha-1/2}(2 - v)^{\alpha-1/2}. \quad (\text{D8})$$

Returning back to the variable $v = 1 + \frac{\mu x}{v_0}$ and using the reflection formula $\Gamma(1/2 + \alpha)\Gamma(1/2 - \alpha) = \pi/\cos(\pi\alpha)$, one finally finds

$$p_X(x) = \frac{\mu}{v_0} \frac{\Gamma(1 + \alpha)}{\sqrt{\pi}\Gamma(1/2 + \alpha)} \left[1 - \left(\frac{\mu x}{v_0} \right)^2 \right]^{\alpha-1/2}, \quad |x| < \frac{v_0}{\mu}, \quad (\text{D9})$$

which is the formula given in Eq. (65) in the main text.

Appendix E: Stationary State Distribution for a Three-State RTP

In this appendix, we provide an illustrative and nontrivial example of a discrete state RTP model, as presented in Section VI. Let us indeed consider a model with $N = 3$ states

$$W(v) = p_1\delta(v - v_1) + p_2\delta(v - v_2) + p_3\delta(v - v_3), \quad (\text{E1})$$

where $v_3 > v_2 > v_1$ and $p_1 + p_2 + p_3 = 1$. In this case, we start with the exact stationary state PDF given in Eq. (119) where we integrate explicitly over the variables z_1 and z_2 . We obtain, for $v_1/\mu < x < v_3/\mu$ simplifies to

$$\begin{aligned} p_X(x) &= \frac{\Gamma(\alpha)}{\Gamma(\alpha p_1)\Gamma(\alpha p_2)\Gamma(\alpha p_3)} \frac{\mu}{v_2 - v_1} \int_{z_3^-}^{z_3^+} dz_3 \left(1 - \frac{\mu x - v_1 - z_3(v_3 - v_1)}{v_2 - v_1} - z_3 \right)^{\alpha p_1 - 1} \\ &\quad \times \left(\frac{\mu x - v_1 - z_3(v_3 - v_1)}{v_2 - v_1} \right)^{\alpha p_2 - 1} z_3^{\alpha p_3 - 1}, \end{aligned} \quad (\text{E2})$$

where we have introduced

$$z_3^- = \max\left(0, \frac{\mu x - v_2}{v_3 - v_2}\right), \quad z_3^+ = \frac{\mu x - v_1}{v_3 - v_1}. \quad (\text{E3})$$

To proceed, we note that the integral over z_3 can be rewritten as follows

$$p_X(x) = \frac{\Gamma(\alpha)}{\Gamma(\alpha p_1)\Gamma(\alpha p_2)\Gamma(\alpha p_3)} \frac{\mu}{v_2 - v_1} \left(\frac{v_2 - \mu x}{v_2 - v_1} \right)^{\alpha p_1 - 1} \left(\frac{\mu x - v_1}{v_2 - v_1} \right)^{\alpha p_2 - 1} I(z_3^-, z_3^+), \quad (\text{E4})$$

with

$$I(z_3^-, z_3^+) = \int_{z_3^-}^{z_3^+} dz_3 \left[1 + \left(\frac{v_3 - v_2}{v_2 - \mu x} \right) z_3 \right]^{\alpha p_1 - 1} \left[1 + \left(\frac{v_3 - v_1}{v_1 - \mu x} \right) z_3 \right]^{\alpha p_2 - 1} z_3^{\alpha p_3 - 1} \quad (\text{E5})$$

$$= \frac{z_3^{\alpha p_3}}{\alpha p_3} F_1 \left(\alpha p_3; 1 - \alpha p_1, 1 - \alpha p_2; \alpha p_3 + 1; \frac{v_3 - v_2}{\mu x - v_2} z, \frac{v_3 - v_1}{\mu x - v_1} z \right) \Big|_{z=z_3^-}^{z=z_3^+}, \quad (\text{E6})$$

where F_1 is the Appell hypergeometric function [95]. Interestingly, because of the singular dependence of z_3^- on x in Eq. (E3), the function $p_X(x)$ takes different functional forms on the intervals $x \in [v_1/\mu, v_2/\mu]$ (where $z_3^- = 0$) and $x \in [v_2/\mu, v_3/\mu]$ (where $z_3^- = (\mu x - v_2)/(v_3 - v_2)$).

Region I: $x \in [v_1/\mu, v_2/\mu]$. In this region, the boundaries of the integral are

$$z_3^- = 0, \quad z_3^+ = \frac{\mu x - v_1}{v_3 - v_1}. \quad (\text{E7})$$

This leads to

$$p_X(x) = \frac{\Gamma(\alpha)}{\Gamma(\alpha p_1)\Gamma(\alpha p_2)\Gamma(\alpha p_3)} \frac{\mu}{v_2 - v_1} \left(\frac{v_2 - \mu x}{v_2 - v_1} \right)^{\alpha p_1 - 1} \left(\frac{\mu x - v_1}{v_2 - v_1} \right)^{\alpha p_2 - 1} \left(\frac{\mu x - v_1}{v_3 - v_1} \right)^{\alpha p_3} \frac{1}{\alpha p_3} \\ \times F_1 \left(\alpha p_3; 1 - \alpha p_1, 1 - \alpha p_2; \alpha p_3 + 1; \frac{v_3 - v_2}{\mu x - v_2} \frac{\mu x - v_1}{v_3 - v_1}, 1 \right). \quad (\text{E8})$$

Region II: $x \in [v_2/\mu, v_3/\mu]$. Here, the boundaries (E3) read

$$z_3^- = \frac{\mu x - v_2}{v_3 - v_2}, \quad z_3^+ = \frac{\mu x - v_1}{v_3 - v_1}. \quad (\text{E9})$$

We obtain

$$p_X(x) = \frac{\Gamma(\alpha)}{\Gamma(\alpha p_1)\Gamma(\alpha p_2)\Gamma(\alpha p_3)} \frac{\mu}{v_2 - v_1} \left(\frac{v_2 - \mu x}{v_2 - v_1} \right)^{\alpha p_1 - 1} \left(\frac{\mu x - v_1}{v_2 - v_1} \right)^{\alpha p_2 - 1} \frac{1}{\alpha p_3} \\ \times \left[\left(\frac{\mu x - v_1}{v_3 - v_1} \right)^{\alpha p_3} F_1 \left(\alpha p_3; 1 - \alpha p_1, 1 - \alpha p_2; \alpha p_3 + 1; \frac{v_3 - v_2}{\mu x - v_2} \frac{\mu x - v_1}{v_3 - v_1}, 1 \right) \right. \\ \left. - \left(\frac{\mu x - v_2}{v_3 - v_2} \right)^{\alpha p_3} F_1 \left(\alpha p_3; 1 - \alpha p_1, 1 - \alpha p_2; \alpha p_3 + 1; 1, \frac{v_3 - v_1}{\mu x - v_1} \frac{\mu x - v_2}{v_3 - v_2} \right) \right]. \quad (\text{E10})$$

In Fig. 11, we compare our theoretical prediction with simulation results.

[1] M. C. Marchetti, J. F. Joanny, S. Ramaswamy, T. B. Liverpool, J. Prost, M. Rao, R. Aditi Simha, *Hydrodynamics of soft active matter*, *Rev. Mod. Phys.* **85**, 3 1143 (2013).
[2] S. Ramaswamy, *Active matter*, *J. Stat. Mech.* **054002** (2017).
[3] E. Fodor, M. Cristina Marchetti, *The statistical physics of active matter: From self-catalytic colloids to living cells*, *Physica A* **504**, 106 (2018).
[4] F. Schweitzer, *Brownian Agents and Active Particles: Collective Dynamics in the Natural and Social Sciences*, Springer: Complexity, Berlin (2003).
[5] L. Gentile, C. Kurzthaler, H. A. Stone, *What is ‘Active Matter’?* in Out-of-equilibrium Soft Matter, ed. C. Kurzthaler, L. Gentile, and H. A. Stone, The Royal Society of Chemistry ch. 1, 1 (2023).

- [6] G. Gompper *et al.*, *J. Phys. Condens. Matter* **37**, 143501 (2025).
- [7] J. Toner, Y. Tu, S. Ramaswamy, *Hydrodynamics and phases of flocks*, *Ann. Phys.* **318**, 170 (2005).
- [8] N. Kumar, H. Soni, S. Ramaswamy, A. K. Sood, *Flocking at a distance in active granular matter*, *Nat. Commun.* **5**, 4688 (2014).
- [9] J. Schwarz-Linek, C. Valeriani, A. Cacciuto, M. E. Cates, D. Marenduzzo, A. N. Morozov, W. C. K. Poon, *Phase separation and rotor self-assembly in active particle suspensions*, *Proc. Natl. Acad. Sci. USA* **109**, 4052 (2012).
- [10] G. S. Redner, M. F. Hagan, A. Baskaran, *Structure and Dynamics of a Phase-Separating Active Colloidal Fluid*, *Phys. Rev. Lett.* **110**, 055701 (2013).
- [11] J. Stenhammar, R. Wittkowski, D. Marenduzzo, M. E. Cates, *Activity-Induced Phase Separation and Self-Assembly in Mixtures of Active and Passive Particles*, *Phys. Rev. Lett.* **114**, 018301 (2015).
- [12] J. O’Byrne, A. Solon, J. Tailleur, Y. Zhao, *An introduction to motility-induced phase separation*, in *Out-of-equilibrium Soft Matter*, ed. C. Kurzthaler, L. Gentile, and H. A. Stone, *The Royal Society of Chemistry*, ch. 4, 107 (2023).
- [13] C. Bechinger, R. Di Leonardo, H. Löwen, C. Reichhardt, G. Volpe, G. Volpe, *Active particles in complex and crowded environments*, *Rev. Mod. Phys.* **88**, 4 045006 (2016).
- [14] P. Denissenko, V. Kantsler, D. J. Smith, J. Kirkman-Brown, *Human spermatozoa migration in microchannels reveals boundary-following navigation*, *Proc. Natl. Acad. Sci. U.S.A.*, **109**, 8007 (2012).
- [15] T. Bhattacharjee, S. S. Datta, *Confinement and activity regulate bacterial motion in porous media*, *Soft Matter* **15**, 9920 (2019).
- [16] S. E. Spagnolie, E. Lauga, *Hydrodynamics of self-propulsion near a boundary: predictions and accuracy of far-field approximations* *J. Fluid Mech.* **700**, 105 (2012).
- [17] Z. Xiao, M. Wei, W. Wang, *A review of micromotors in confinements: Pores, channels, grooves, steps, interfaces, chains, and swimming in the bulk*, *ACS Appl. Mater. Interfaces* **11**, 6667 (2018).
- [18] H. Wioland, F. G. Woodhouse, J. Dunkel, J. O. Kessler, R. E. Goldstein, *Confinement stabilizes a bacterial suspension into a spiral vortex*, *Phys. Rev. Lett.* **110**, 268102 (2013).
- [19] A. P. Berke, L. Turner, H. C. Berg, E. Lauga, *Hydrodynamic Attraction of Swimming Microorganisms by Surfaces*, *Phys. Rev. Lett.* **101**, 038102 (2008).
- [20] J. Tailleur, M. E. Cates, *Sedimentation, trapping, and rectification of dilute bacteria*, *EPL* **86**, 60002 (2009).
- [21] A. Pototsky, H. Stark, *Active Brownian particles in two-dimensional traps*, *EPL* **98**, 50004 (2012).
- [22] A. P. Solon, M. E. Cates, J. Tailleur, *Active brownian particles and run-and-tumble particles: A comparative study*, *Eur. Phys. J.: Spec. Top.* **224**, 1231 (2015).
- [23] L. Angelani, R. Garra, *Run-and-tumble motion in one dimension with space-dependent speed*, *Phys. Rev. E* **100**, 052147 (2019).
- [24] A. Dhar, A. Kundu, S. N. Majumdar, S. Sabhapandit, G. Schehr, *Run-and-tumble particle in one-dimensional confining potential: Steady state, relaxation and first passage properties*, *Phys. Rev. E*, **99**, 032132 (2019).
- [25] K. Goswami, K. L. Sebastian, *Diffusion caused by two noises - active and thermal*, *J. Stat. Mech.* **083501** (2019).
- [26] P. C. Bressloff, *Encounter-based model of a run-and-tumble particle*, *J. Stat. Mech.* **113206** (2022).
- [27] N. R. Smith, O. Farago, *Nonequilibrium steady state for harmonically confined active particles*, *Phys. Rev. E* **106**, 054118 (2022).
- [28] P. Romanczuk, M. Bär, W. Ebeling, B. Lindner, L. Schimansky-Geier, *Active Brownian particles: From individual to collective stochastic dynamics*, *Eur. Phys. J. Spec. Top.* **202**, 1 (2012).
- [29] C. Kurzthaler, S. Leitmann, T. Franosch, *Intermediate scattering function of an anisotropic active Brownian particle*, *Sci. Rep.* **6**, 36702 (2016).
- [30] U. Basu, S. N. Majumdar, A. Rosso, G. Schehr, *Active Brownian motion in two dimensions*, *Phys. Rev. E* **98**, 062121 (2018).
- [31] U. Basu, S. N. Majumdar, A. Rosso, G. Schehr, *Long time position distribution of an active Brownian particle in two dimensions*, *Phys. Rev. E* **100**, 062116 (2019).
- [32] L. L. Bonilla, *Active Ornstein-Uhlenbeck particles*, *Phys. Rev. E* **100**, 022601 (2019).
- [33] D. Martin, J. O’Byrne, M. E. Cates, E. Fodor, C. Nardini, J. Tailleur, F. van Wijland, *Statistical mechanics of active Ornstein-Uhlenbeck particles*, *Phys. Rev. E* **103**, 032607 (2021).
- [34] J. Tailleur, M. E. Cates, *Statistical mechanics of interacting run-and-tumble bacteria*, *Phys. Rev. Lett.* **100**, 218103 (2008).
- [35] K. Malakar, V. Jemseena, A. Kundu, K. Vijay Kumar, S. Sabhapandit, S. N. Majumdar, S. Redner, A. Dhar, *Steady state, relaxation and first-passage properties of a run-and-tumble particle in one-dimension*, *J. Stat. Mech.* **043215** (2018).
- [36] G. H. Weiss, *Some applications of persistent random walks and the telegrapher’s equation*, *Physica A* **311**, 381 (2002).
- [37] M. Caraglio, T. Franosch, *Analytic Solution of an Active Brownian Particle in a Harmonic Well*, *Phys. Rev. Lett.* **129**, 158001 (2022).
- [38] K. Malakar, A. Das, A. Kundu, K. Vijay Kumar, A. Dhar, *Steady State of an Active Brownian Particle in Two-Dimensional Harmonic Trap*, *Phys. Rev. E* **101**, 022610 (2020).
- [39] D. Frydel, *Positing the problem of stationary distributions of active particles as third-order differential equation*, *Phys. Rev. E*, **106** 024121 (2022).
- [40] D. Frydel, *Run-and-tumble oscillator: Moment analysis of stationary distributions*, *Physics of Fluids* **35** (2023).
- [41] D. Frydel, *Integral equation formulation of run-and-tumble particles in a harmonic trap: special status of a system in two-dimensions*, *New J. Phys.* **27** 074601 (2025).
- [42] D. Frydel, *The run-and-tumble particle model with four-states: Exact solution at zero temperature*, *Phys. Fluids* **34**, 027111 (2022).

[43] H. C. Berg, *E. coli in Motion*, Springer Verlag, Heidelberg, Germany (2004).

[44] H. C. Berg, D. A. Brown, *Chemotaxis in Escherichia coli analysed by three-dimensional tracking*, *Nature* **239**, 500 (1972).

[45] C. Kurzthaler, Y. Zhao, N. Zhou, J. Schwarz-Linek, C. Devailly, J. Arlt, J. D. Huang, W. C. K. Poon, T. Franosch, J. Tailleur, V. A. Martinez, *Characterization and control of the run-and-tumble dynamics of Escherichia coli*, *Phys. Rev. Lett.* **132**, 038302 (2024).

[46] Y. Zhao, C. Kurzthaler, N. Zhou, J. Schwarz-Linek, C. Devailly, J. Arlt, J. D. Huang, W. C. K. Poon, T. Franosch, V. A. Martinez, J. Tailleur, *Quantitative characterization of run-and-tumble statistics in bulk bacterial suspensions*, *Phys. Rev. E* **109**, 014612 (2024).

[47] K. Martens, L. Angelani, R. Di Leonardo, L. Bocquet, *Probability distributions for the run-and-tumble bacterial dynamics: An analogy to the Lorentz model*, *Eur. Phys. J. E* **35**, 84 (2012).

[48] L. Angelani, *Averaged run-and-tumble walks*, *Eur. Phys. Lett.* **102**, 20004 (2013).

[49] P. Singh, A. Kundu, *Generalised 'Arcsine' laws for run-and-tumble particle in one dimension*, *J. Stat. Mech.* 083205 (2019).

[50] F. Mori, P. Le Doussal, S. N. Majumdar, G. Schehr, *Universal properties of a run-and-tumble particle in arbitrary dimension*, *Phys. Rev. E* **102**, 042133 (2020).

[51] F. Mori, P. Le Doussal, S. N. Majumdar and G. Schehr, *Universal Survival Probability for a d-Dimensional Run-and-Tumble Particle*, *Phys. Rev. Lett.* **124**, 090603 (2020).

[52] F. Mori, P. Le Doussal, S. N. Majumdar and G. Schehr, *Condensation transition in the late-time position of a run-and-tumble particle*, *Phys. Rev. E*, **103**, 062134 (2021).

[53] B. De Bruyne, S. N. Majumdar, G. Schehr, *Survival probability of a run-and-tumble particle in the presence of a drift*, *J. Stat. Mech.* 043211 (2021).

[54] M. Guéneau, S. N. Majumdar, G. Schehr, *Run-and-tumble particle in one-dimensional potentials: mean first-passage time and applications*, *Phys. Rev. E* **111**, 014144 (2025).

[55] M. Guéneau, S. N. Majumdar, G. Schehr, *Optimal mean first-passage time of a run-and-tumble particle in a class of one-dimensional confining potential*, *EPL* **145**, 61002 (2024).

[56] M. Guéneau, L. Touzo, *Relating absorbing and hard wall boundary conditions for active particles*, *J. Phys. A: Math. Theor.* **57**, 225005 (2024).

[57] S. K. Nath, S. Sabhapandit, *Survival probability and position distribution of a run and tumble particle in $U(x) = \alpha|x|$ potential with an absorbing boundary*, *J. Stat. Mech.* 093205 (2024).

[58] P. Grange, L. Yuan, *Mean first-passage time at the origin of a run-and-tumble particle with periodic forces*, *preprint arXiv:2411.11601*.

[59] Y. Ben Dor, E. Woillez, Y. Kafri, M. Kardar, A. P. Solon, *Ramifications of disorder on active particles in one dimension*, *Phys. Rev. E*, **100**, 052610 (2019).

[60] V. Tejedor, R. Voituriez, O. Bénichou, *Optimizing persistent random searches*, *Phys. Rev. Lett.* **108**, 088103 (2012).

[61] J.-F. Rupprecht, O. Bénichou, R. Voituriez, *Optimal search strategies of run-and-tumble walks*, *Phys. Rev. E* **94**, 012117 (2016).

[62] L. Angelani, *Optimal escapes in active matter*, *Eur. Phys. J. E* **47**, 9 (2024).

[63] L. Angelani, R. Di Leonardo, M. Paoluzzi, *First-passage time of run-and-tumble particles*, *Eur. J. Phys. E* **37**, 59 (2014).

[64] U. Basu, S. Sabhapandit, and I. Santra, *Target search by active particles*, In *Target Search Problems* (pp. 463-487). Cham: Springer Nature Switzerland (2024).

[65] P. C. Bressloff, *Encounter-based model of a run-and-tumble particle II: absorption at sticky boundaries*, *J. Stat. Mech.* 043208 (2023).

[66] A. Ashkin, *Acceleration and trapping of particles by radiation pressure* *Phys. Rev. Lett.*, **24** 156 (1970).

[67] R. Diekmann, D. L. Wolfson, C. Spahn, M. Heilemann, M. Schüttelz, T. Huser, *Nanoscopy of bacterial cells immobilized by holographic optical tweezers*, *Nat. Commun.* **7**, 13711 (2016).

[68] A. Ashkin, J. M. Dziedzic, *Optical trapping and manipulation of viruses and bacteria*, *Science* **235** 1517 (1987).

[69] T. L. Min, P. J. Mears, L. M. Chubiz, C. V. Rao, I. Golding, Y. R. Chemla, *High-resolution, long-term characterization of bacterial motility using optical tweezers* *Nature methods*, **6** 831-835 (2009).

[70] S. C. Takatori, R. De Dier, J. Vermant, J. F. Brady, *Acoustic trapping of active matter*, *Nat. Commun.*, **7** 10694 (2016).

[71] M. Guéneau, S. N. Majumdar, G. Schehr, *Active particle in a harmonic trap driven by a resetting noise: an approach via Kesten variables*, *J. Phys. A: Math. Theor.* **56**, 475002 (2023).

[72] U. Basu, S. N. Majumdar, A. Rosso, S. Sabhapandit, G. Schehr, *Exact stationary state of a run-and-tumble particle with three internal states in a harmonic trap*, *J. Phys. A: Math. Theor.* **53**, 9 (2020).

[73] N. R. Smith, P. Le Doussal, S. N. Majumdar, G. Schehr, *Exact position distribution of a harmonically confined run-and-tumble particle in two dimensions* *Phys. Rev. E* **106**, 054133 (2022).

[74] H. Kesten, *Random difference equations and renewal theory for products of random matrices*, *Acta Math.* **131**, 207 (1973).

[75] D. M. Cifarelli, E. Regazzini, *Distribution functions of means of a Dirichlet process*, *Ann. Stat.* **18**, 429 (1990).

[76] T. S. Ferguson, *A Bayesian analysis of some nonparametric problems*, *Ann. Stat.* **1**, 209 (1973).

[77] J. Sethuraman, *A constructive definition of Dirichlet priors*, *Stat. Sin.* **4**, 639 (1994).

[78] P. Le Doussal, S. N. Majumdar, G. Schehr, *Velocity and diffusion constant of an active particle in a one-dimensional force field*, *EPL* **130**, 40002 (2020).

[79] L. Hahn, *A General Approach to the Shape Transition of Run-and-Tumble Particles: The 1D PDMP Framework for Invariant Measure Regularity*, *arXiv:2506.02274*

[80] T. Herbeau, L. Pastur, P. Viot and G. Oshanin, *A General Approach to the Shape Transition of Run-and-Tumble Particles: The 1D PDMP Framework for Invariant Measure Regularity*, *J. Stat. Mech.* 013205 (2025).

- [81] L. Comtet, Advanced Combinatorics: The art of finite and infinite expansions. Springer Science & Business Media, (2012).
- [82] https://en.wikipedia.org/wiki/Bell_polytomial
- [83] V I. Klyatskin, *Dynamic systems with parameter fluctuations of the telegraphic-process type*, Radiophys. Quantum El. **20**, 382 (1977).
- [84] R. Lefever, W. Horsthemke, K. Kitahara, I. Inaba, *Phase Diagrams of Noise Induced Transitions: Exact Results for a Class of External Coloured Noise*, Prog. Theor. Phys. **64**, 1233 (1980).
- [85] J. Tailleur and M. E. Cates, *Sedimentation, trapping, and rectification of dilute bacteria*, Europhys. Lett. **86**, 60002 (2009).
- [86] M. Guéneau, *Non-Equilibrium Dynamics and First-Passage Properties of Stochastic Processes : From Brownian Motion to Active Particles*, Sorbonne Université (2025).
- [87] C. Godrèche, J. M. Luck, *A record-driven growth process*, Journal of Statistical Mechanics: Theory and Experiment, 2008 P11006 (2008).
- [88] P. J. Forrester, *Log-gases and random matrices* (LMS-34) Princeton university press (2010).
- [89] S. Sabhapandit, S. N. Majumdar, *Noninteracting particles in a harmonic trap with a stochastically driven center*, J. Phys. A: Math. Theor. **57**, 335003 (2024).
- [90] N. C. Darnton, L. Turner, S. Rojevsky, H. C. Berg, *On torque and tumbling in swimming Escherichia coli*, Journal of bacteriology, **189**(5), 1756-1764 (2007).
- [91] K. Taute, S. Gude, S. J. Tans, T. S. Shimizu, *High-throughput 3D tracking of bacteria on a standard phase contrast microscope*, Nat Commun **6**, 8776 (2015).
- [92] M. Guéneau, S. N. Majumdar, G. Schehr, *Large Deviations in Switching Diffusion: from Free Cumulants to Dynamical Transitions*, Phys. Rev. Lett. **135**, 067102 (2025).
- [93] M. Biroli, M. Kulkarni, S. M. Majumdar, G. Schehr, *Dynamically emergent correlations between particles in a switching harmonic trap*, Phys. Rev. E **109**, L032106 (2024).
- [94] M. Biroli, S. Ciliberto, M. Kulkarni, S. N. Majumdar, A. Petrosyan, G. Schehr, Experimental evidence for strong emergent correlations between particles in a switching trap. arXiv:2508.07199.
- [95] https://en.wikipedia.org/wiki/Appell_series